V. Heavy Quark Production

V.1 Quarkonia in e^+e^- Collisions

- e^+e^- annihilation (s-channel) is the classic channel for production & study of heavy quarks as cross sections are relatively large wrt backgrounds
- A $(Q\bar{Q})$ bound state with zero net flavor is called quarkonium of which some are directly produced as narrow resonances in e^+e^- collisions
- *c*-quarks were simultaneously discovered in e^+e^- collisions & *p*-*N* collisions via the J/ψ resonance
- *b*-quarks were discovered in *p*-*N* collisions via the Υ resonance, but for exploration they were produced at e^+e^- colliders
- Note that no resonance was found in *t*-quark production, because due to V_{tb}=1 the t-quark decays before forming a $t\bar{t}$ bound state
- In a heavy $(Q\bar{Q})$ system many possible states can be produced
- In a non-relativistic approximation the total angular momentum of the $(Q\bar{Q})$ system is $\vec{J} = \vec{L} + \vec{S}$ with spin $\vec{S}$=0 (antisymmetric) & $\vec{S}$=1 (symmetric
- Parity & *C*-parity of the system are $P=(-1)^{L+1}$ and $C=(-1)^{L+S}$

V.1.1 ($Q\bar{Q}$) in e^+e^- Collisions: Properties

- We introduce the following notation

	S=0	S=1	$^{2S+1}L_J$
L=0	η_Q (0^{-+})	ψ, Υ (1^{--})	$^1S_0$ $^3S_1$
L=1	h_Q (1^{+-})	χ_J (0^{++}, 1^{++}, 2^{++})	$^1P_1$ ^3P_J
L=2	2^{-+}	1^{--}, 2^{--}, 3^{--}	$^1D_2$ ^3D_J

- Only $J^{PC}=1^-$ states can be produced in e^+e^- annihilation via a virtual photon
- In principle $J^{PC}=1^{++}$ states could be produced by virtual Z^0 axial vector coupling, but that it is suppressed by the angular momentum barrier
- For production of 1^{--} states we can apply the cross section formulae from the previous chapter
- Since e^+ & e^- beam energy resolutions are much larger than the natural resonance width, we have to use the energy-integrated formulae here

$$\int d\sqrt{s}\,\sigma(e^+e^- \to \Upsilon \to X) = \frac{6\pi^2}{M_V^2}\frac{\Gamma_{ee}\Gamma_X}{\Gamma} \qquad (5.1)$$

where X denotes any particular set of final states, Γ_X denotes corresponding partial width and Γ is the total width

V.1.2 $(Q\bar{Q})$ in e^+e^- Collisions: Potential

- Note that the total integrated cross section is proportional to Γ_{ee}
- The production cross section and the annihilation decay width of $^3S_1$ quarkonia are determined by the wave function at the origin
- The number of narrow $^3S_1$ states below threshold can be estimated in a potential model framework: 2 for $c\bar{c}$ and 3 for $b\bar{b}$
- Quarkonium states with masses above the threshold for producing 2 heavy Q-flavored mesons will decay strongly into the latter (Zweig's rule) and therefore have much larger widths (~10^3 times) than states below this threshold energy
- If we set $E_0=2m_Q$, then the interquark potential $V(r)$ arising from QCD is independent of flavor
- The interquark potential has been parameterized as a sum of 3 contributions

$$V(r) = -\frac{4}{3}\frac{\alpha_s(r)}{r} + V_l(r) + ar \qquad (5.2)$$

- The 1st term is the short-distance Coulomb-like term (the Fourier transform of the 1-gluon exchange scattering amplitude)

V.1,2 ($Q\bar{Q}$) in e^+e^- Collisions: Potential

- $\alpha_s(r)$ is the Fourier transform of $\alpha_s(Q^2)$ but the logarithmic behavior of α_s within the Fourier transform can be included
- At the 2-loop level one finds

$$\alpha_s(r) = \frac{12\pi}{25t}\left[1 - \frac{462}{625}\frac{\ln t}{t} + \left(\frac{57}{75} + 2\gamma_E\right)\frac{1}{t} + \mathcal{O}\left(\frac{1}{t^2}\right)\right] \qquad (5.3)$$

where $t = -\ln\left(r^2\Lambda^2_{\overline{MS}}\right)$, γ_E=0.5772 is Euler's constant and $\Lambda_{\overline{MS}}$ is the QCD scale parameter in the $\overline{MS}$ minimal subtraction scheme

- The 3rd term is the confining potential with $a \approx 0.2$ GeV^2
- The 2nd term $V_I(r)$ parameterizes additional intermediate contributions
- Several parameterizations exist
- Their parameters are fixed by $c\bar{c}$ and $b\bar{b}$ quarkonium data

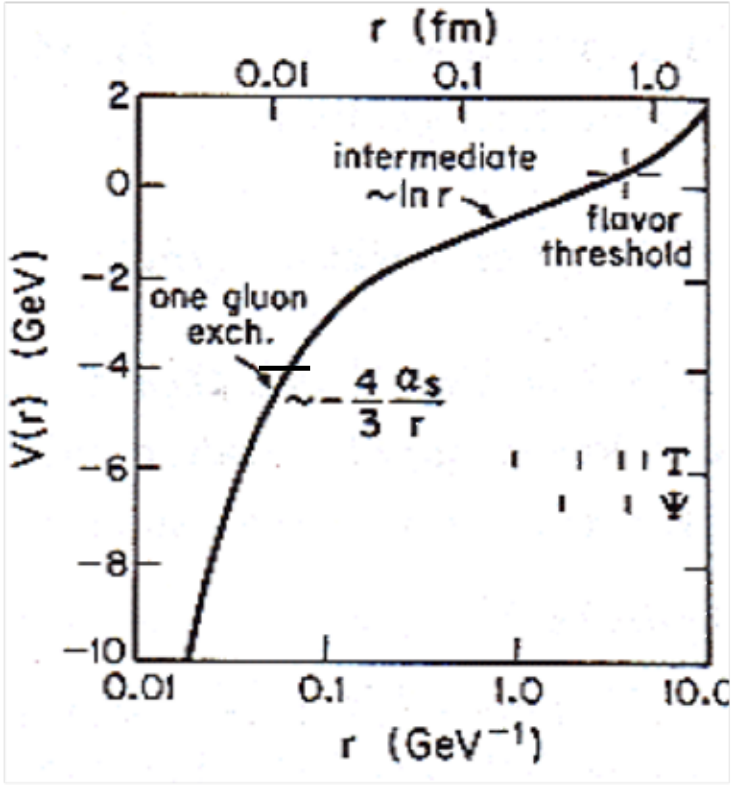

V.1.3 ($Q\bar{Q}$) in e^+e^- Collisions: Matrix Elements

- From the standard results for the hydrogen atom the wave function of the 1-gluon exchange alone with $\alpha_s(m^2_Q)$ gives the L=0 wave functions at the origin as

$$\left|\Psi_n(0)\right|^2 = \frac{1}{\pi}\left[\frac{2}{3}\frac{m_Q}{n}\alpha_s(m_Q^2)\right]^3 \qquad (5.4)$$

  where $\Psi_n(r)$ is the complete wave function & n=1,2 .. is radial QN

- Short distance structure of the wave function of $^3S_1$, quarkonium state $V(QQ)$ is represented by ME

$$\left\langle 0\left|\bar{Q}\gamma^\mu Q\right|\Psi_V\right\rangle = \varepsilon_V^\mu F_V \qquad (5.5)$$

  where <0| is vacuum, ε_V is V polarization & F_V V-decay constant

- The latter can be expressed by the wave function at origin by

$$\left|F_V\right|^2 = 12m_V\left|\Psi_V(0)\right|^2 \qquad (5.6)$$

- Since the $Q\bar{Q}$ state is coupled to γ and Z^0, V is coupled through them to $f\bar{f}$ via an effective ME

$$M(V\to f\bar{f}) = -iF_V\varepsilon_{V\mu}\left[\bar{u}(f)\gamma^\mu\left(G_V^f + G_A^f\gamma_5\right)v(\bar{f})\right] \qquad (5.7)$$

V.1.4 ($Q\bar{Q}$) in e^+e^- Collisions: Decay Widths

with

$$G_V^f = \frac{8G_F M_Z^2}{\sqrt{2}} \frac{g_V^f g_V^Q}{s - M_Z^2 + i\Gamma_Z M_Z} + \frac{e^2 e_f e_Q}{s} \qquad (5.8)$$

$$G_A^f = \frac{8G_F M_Z^2}{\sqrt{2}} \frac{g_A^f g_A^Q}{s - M_Z^2 + i\Gamma_Z M_Z} \qquad (5.9)$$

where e_f, e_Q are fermion & quark charges and g^i_V, g^i_A are couplings of f & Q to the Z^0

- Hence the EM decay width to e^+e^- or $\mu^+\mu^-$ is

$$\Gamma_\gamma = \Gamma(V \to \gamma^* \to e^+e^-) = \frac{4\pi\alpha^2 e_Q^2}{3M_V^3} |F_V|^2 \left[1 - \frac{16}{3\pi}\alpha_s(m_Q^2)\right] \qquad (5.10)$$

- The expression in [ ] is the QCD correction, common to other modes
- For $M_V \ll M_Z$, the virtual photon contribution dominates e^+e^- modes
- The ϕ, ψ, & Υ ground states have a partial width of

$$\Gamma(V \to e^+e^-) \simeq (11\,keV) \cdot e_Q^2 \qquad (5.11)$$

- indicating that $|\Psi_V(0)|^2 \sim m^2_V$ for these states

V.1.4 ($Q\bar{Q}$) in e^+e^- Collisions: Decay Widths

- Note that quarkonium decays are Zweig suppressed ➔ narrow width

- For the virtual γ & Z^0 decay (a) the partial width is

$$\Gamma(V \to f\bar{f}) = C\left(m_V^2/e^2 e_Q\right)^2 \left(\left|G_V^f\right|^2 + \left|G_A^f\right|^2\right)\Gamma_\gamma \qquad (5.12)$$

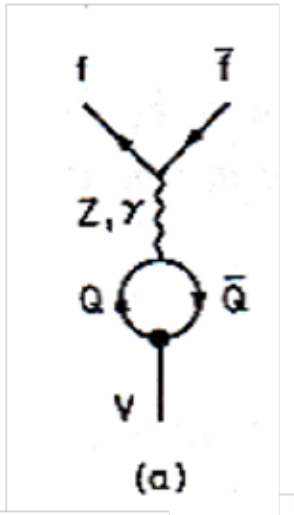

where C=3 (1) for quarks (leptons) is color factor and G_V & G_A are evaluated at $s=M^2_V$

- The *ggg* decay (b) is the dominant mode for ψ & Υ with partial widths

$$\Gamma(V \to ggg) = \frac{10\left(\pi^2 - 9\right)}{81\pi e_Q^2}\frac{\alpha_s^3}{\alpha^2}\Gamma_\gamma \qquad (5.13)$$

- Another large decay is the $gg\gamma$ mode that has a partial width of

$$\Gamma(V \to gg\gamma) = \frac{8\left(\pi^2 - 9\right)}{9\pi}\frac{\alpha_s^2}{\alpha}\Gamma_\gamma \qquad (5.14)$$

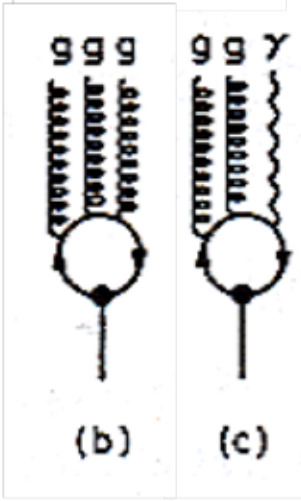

V.1.4 ($Q\bar{Q}$) in e^+e^- Collisions: Decay Widths

- In addition, suppressed decays occur that may become important in case of very heavy ($Q\bar{Q}$) states
- Quarkonium production is signaled by narrow peaks in the total & partial e^+e^- cross sections
- So an $f\bar{f}$ final state is produced via γ or Z^0 transition yielding amplitudes of

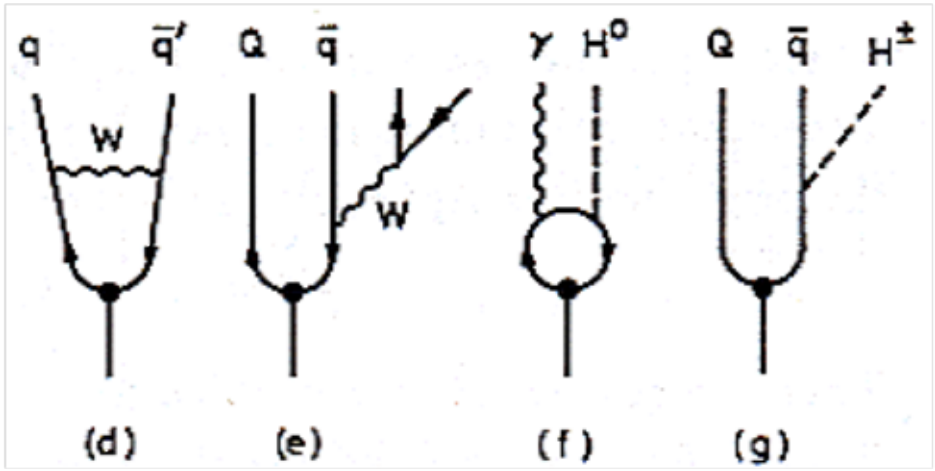

$$M(e^+e^- \to \gamma \to f\bar{f}) = -\frac{4\pi\alpha e_f}{s}\left[\bar{u}(f)\gamma^\mu v(\bar{f})\right]\left[v(e^+)\gamma_\mu u(e^-)\right] \qquad (5.15)$$

$$M(e^+e^- \to V \to f\bar{f}) = \frac{|F_V|^2}{s - M_V^2 + i\Gamma_V M_V}\left[\bar{u}(f)\gamma_\mu\left(G_V^f + G_A^f\gamma_5\right)v(f)\right]\left[\bar{v}(e^+)\gamma^\mu\left(G_V^e + G_A^e\gamma_5\right)u(e^-)\right] \qquad (5.16)$$

- Note that at $s=M^2_\Upsilon$, the direct $e^+e^- \to \gamma \to f\bar{f}$ amplitude does not interfere with the $e^+e^- \to \Upsilon \to f\bar{f}$ amplitude
- We focused here on S-wave quarkonia with S=1 that includes $^3S_1$-$^3D_1$ mixtures
- Other states can be produced by γ & hadron transitions from $^3S_1$ states

V.1.5 ($Q\bar{Q}$) in e^+e^- Collisions: EM Transistions

- Photon transitions in the charmonium and bottomonium system

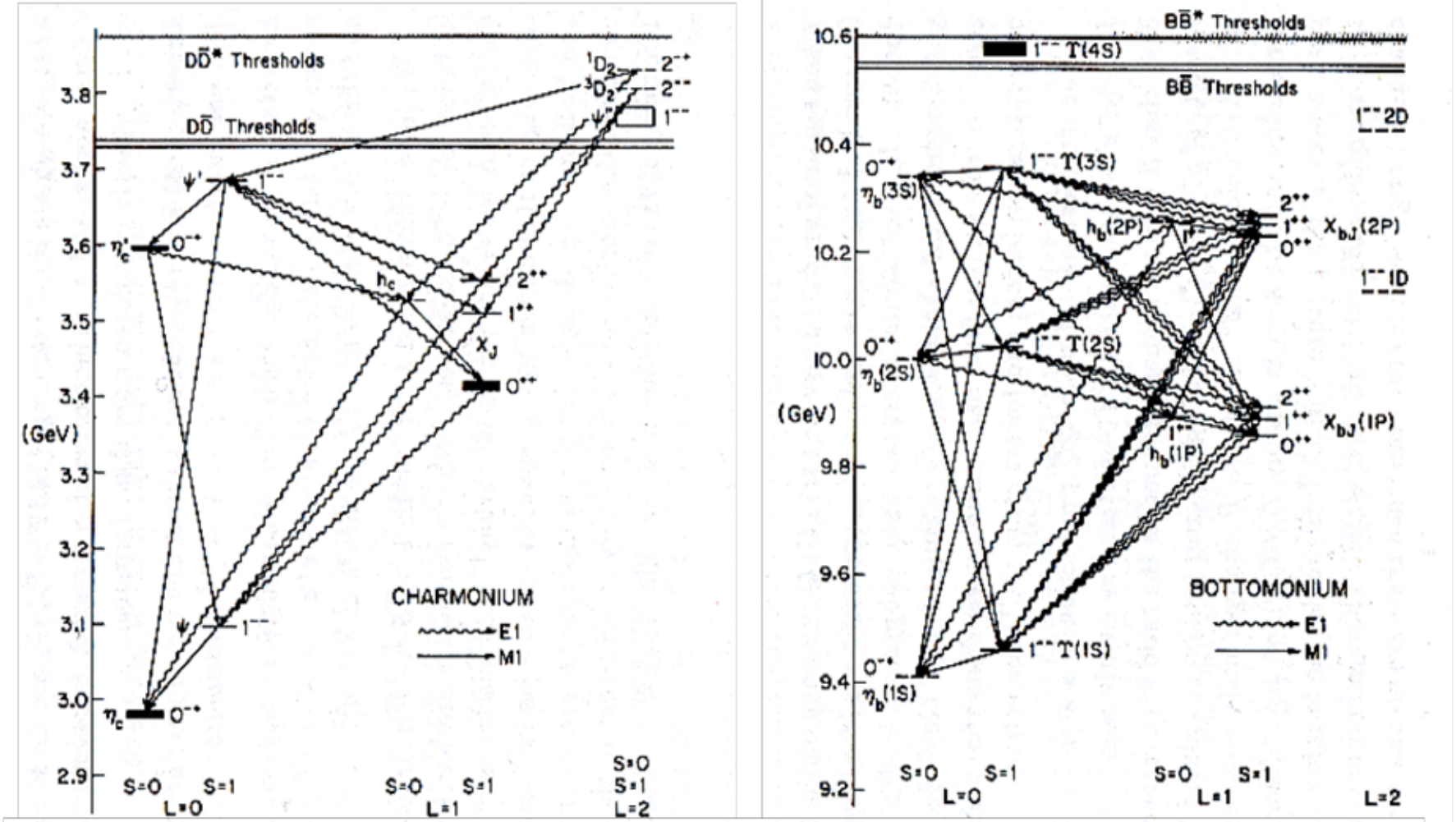

Fig. 10.4. Production of χ, η and h states from electromagnetic decays of ψ and Υ states. Wiggly lines (straight lines) denote E1 (M1) transitions.

V.1.6 ($Q\bar{Q}$) in e^+e^- Collisions: $c\bar{c}$ γ Spectrum

- E.g., in the charmonium system many photon transition have been observed providing access to non $^3S_1$ states

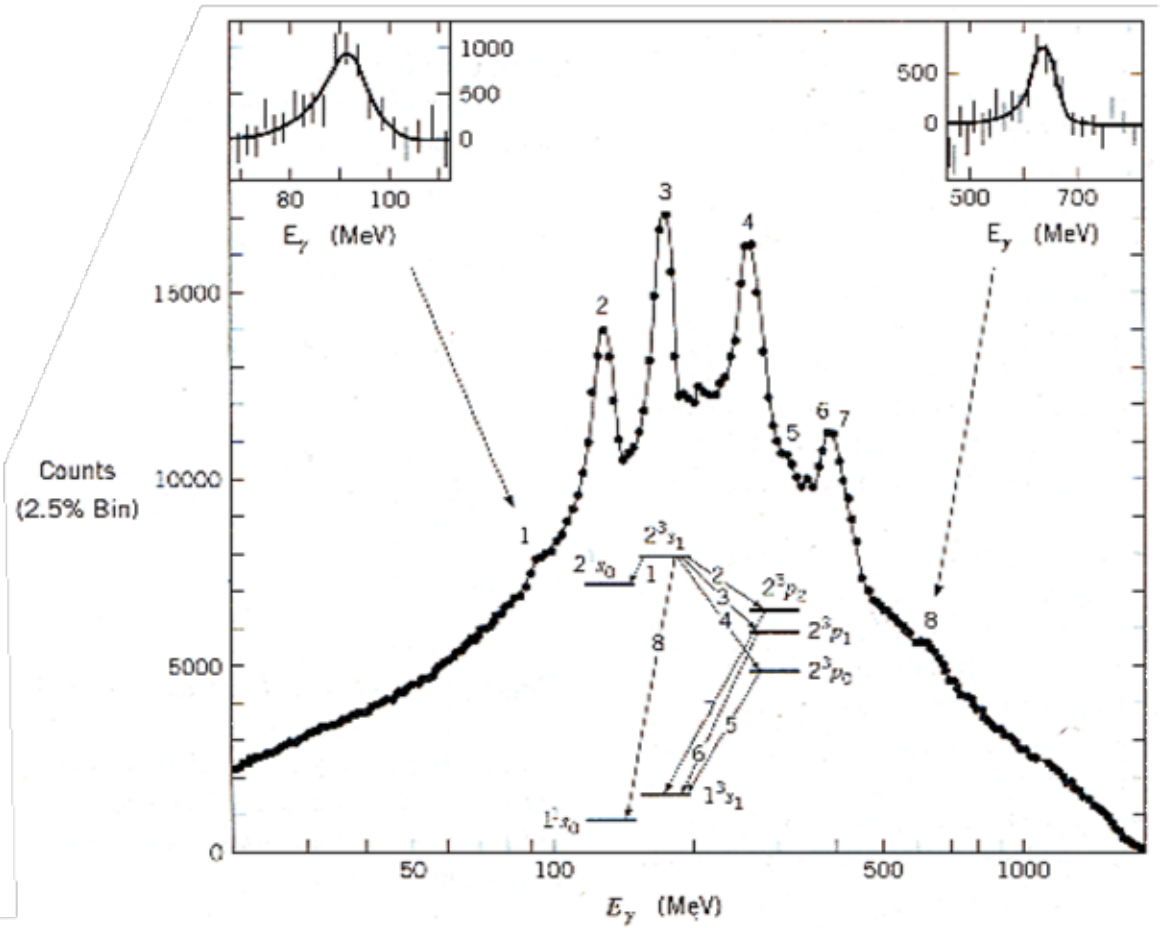

FIGURE 17-18 Measurement of the energy levels of charmonium.
The energies of photons from the $\psi(2s)$ are measured from their electromagnetic interactions in crystals of NaI(Tl). Each photon "line" corresponds to a transition between charmonium energy levels. The inserts show the transitions to the singlet states after the contributions from π^0s are subtracted. From the Crystal Ball Collaboration, reported by E. D. Bloom and C. W. Peck, "Crystal Ball Physics," *Ann. Rev. Nucl. Part. Science* **33**, 143 (1983).

V.1.7 ($Q\bar{Q}$) in e^+e^- Collisions: $b\bar{b}$ γ Spectrum

- In the bottomonium system many photon transition have been also observed to non $^3S_1$ states

$\Upsilon(2S)\to\gamma\chi_{0,1,2}(1P)$ $\Upsilon(3S)\to\gamma\chi_{0,1,2}(2P)$

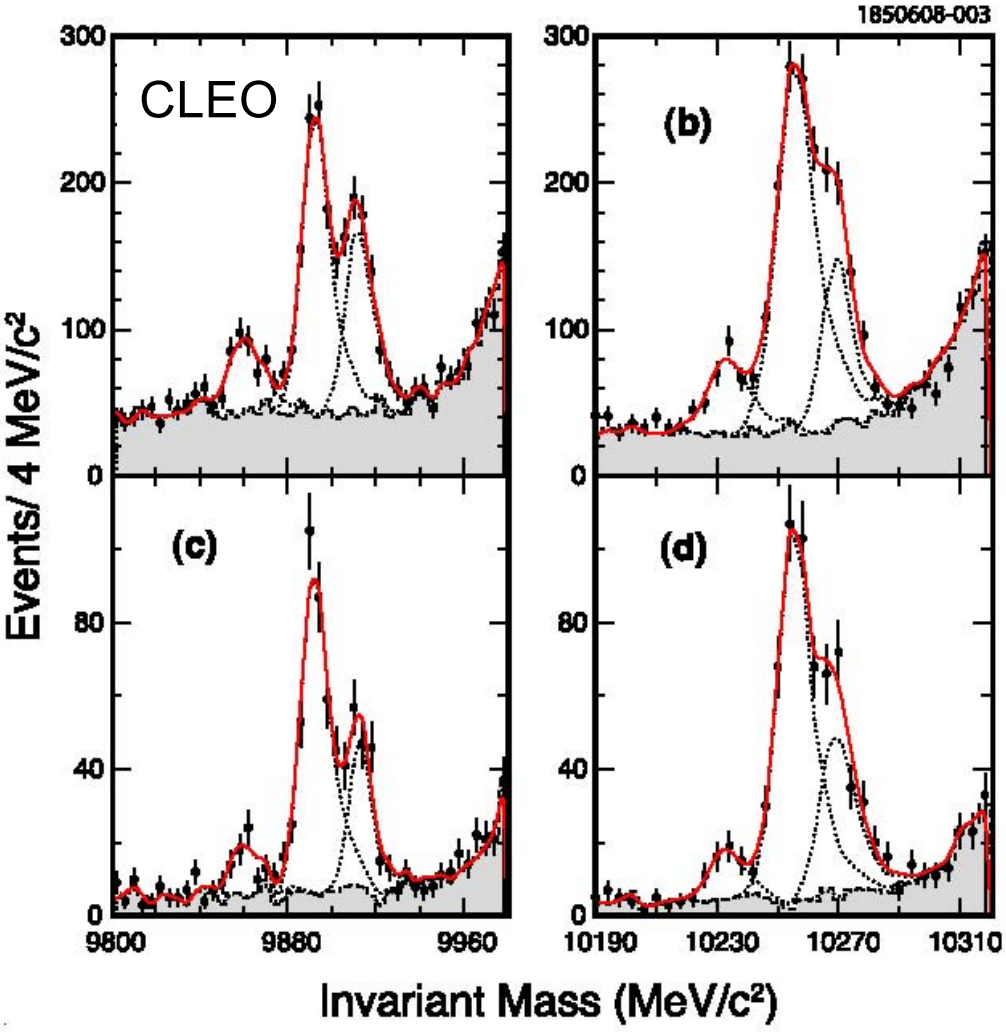

$\Upsilon(2S)\to\gamma\eta_b$

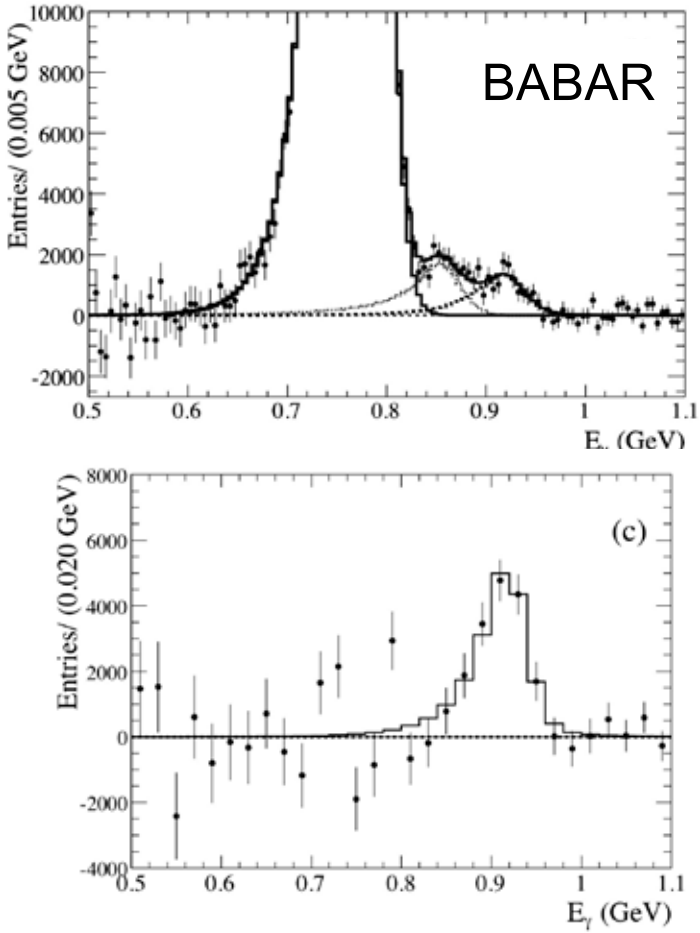

$$m_{\eta_b} = 9388.9^{+3.1}_{-2.3} \pm 2.7 \text{ MeV}$$

(5.17)

V.1.8 ($Q\bar{Q}$) in e^+e^- Collisions: $b\bar{b}$ States

- Study decay $\Upsilon(5S) \rightarrow h_b(nP)\,\pi^+\pi^-$, reconstruct only $p(\pi^+\pi^-)$ and look in missing mass $p(\Upsilon(5S))$- $p(\pi^+\pi^-)$

Belle 2011

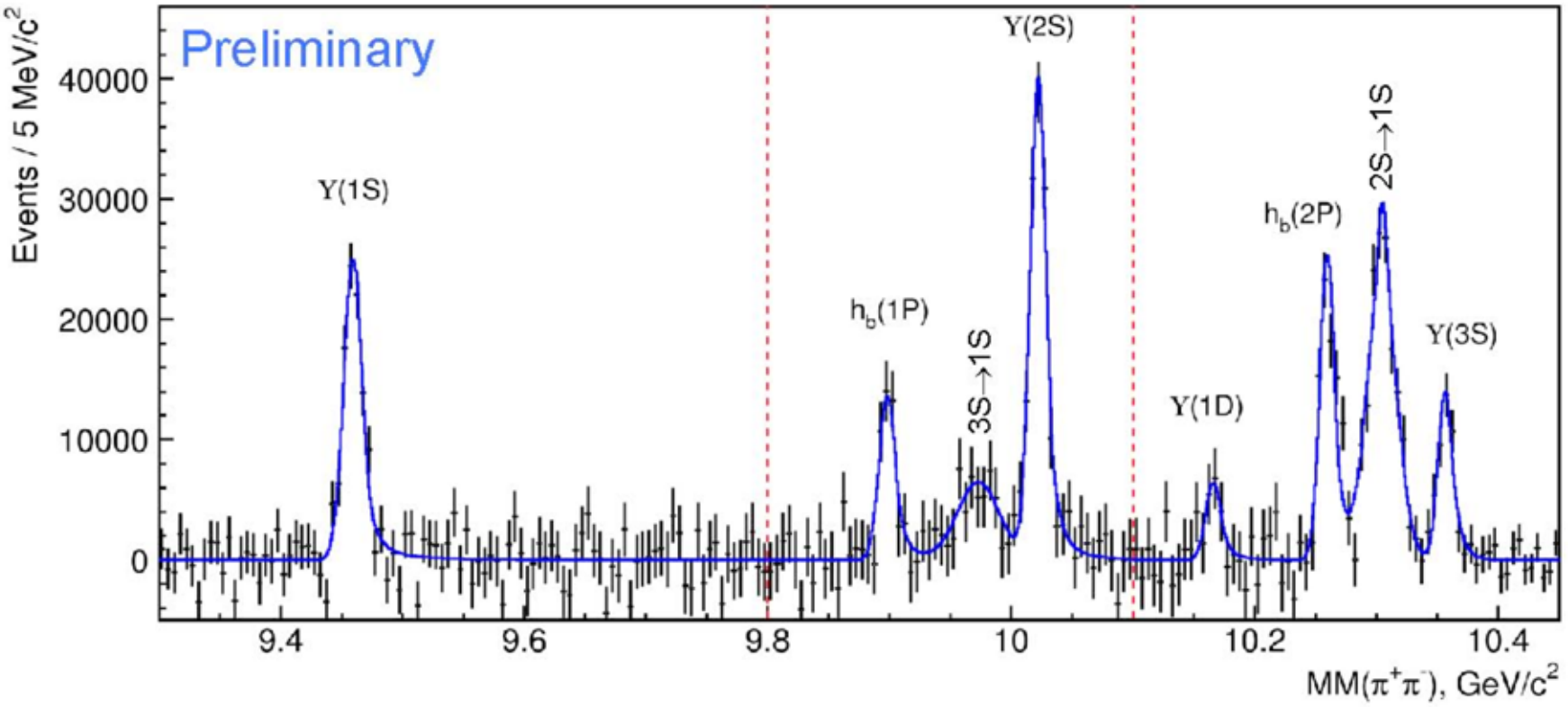

- Observe $h_b(1P)$ and $h_b(2P)$ with significance of 6.2σ and 12.4σ at masses

$$m_{h_b(1P)} = 9898.25 \pm 1.06^{+1.03}_{-1.07}\ \text{MeV} \qquad m_{h_b(2P)} = 10259.76 \pm 0.64^{+1.43}_{-1.03}\ \text{MeV} \qquad (5.18)$$

- BABAR observed the $h_b(1P)$ at the same time in π^0 transitions

V.1.8 ($Q\bar{Q}$) in e^+e^- Collisions: $b\bar{b}$ States

- See new states in decaying to J/ψ
  - $X(3872) \to \pi\pi J/\psi$
    m=(3872±8) MeV, Γ< 2.3 MeV @90%CL
  - In ISR events see $Y(4260) \to J/\psi\pi^+\pi^-$
    m=(4258±8) MeV, Γ=(88±23) MeV
- Nature of these states is not yet clear

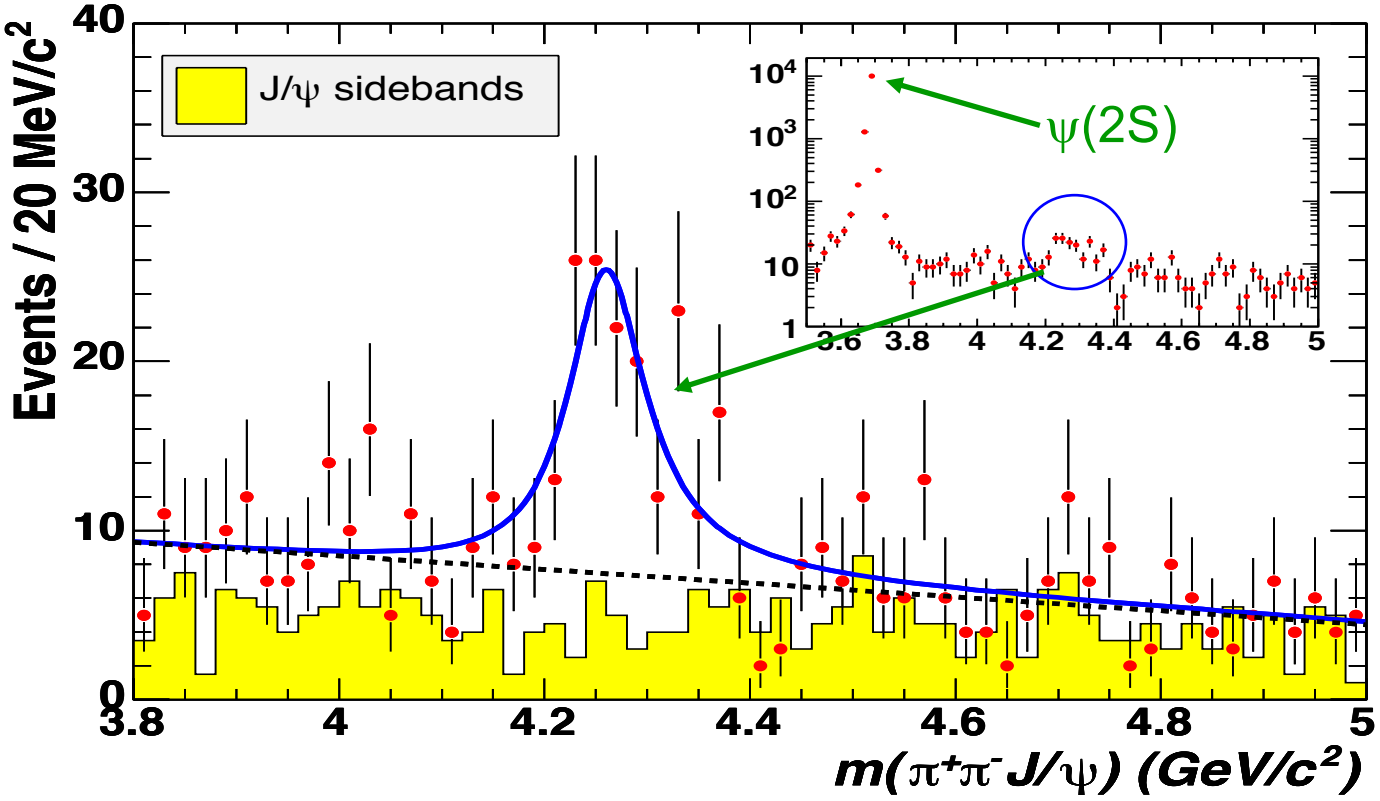

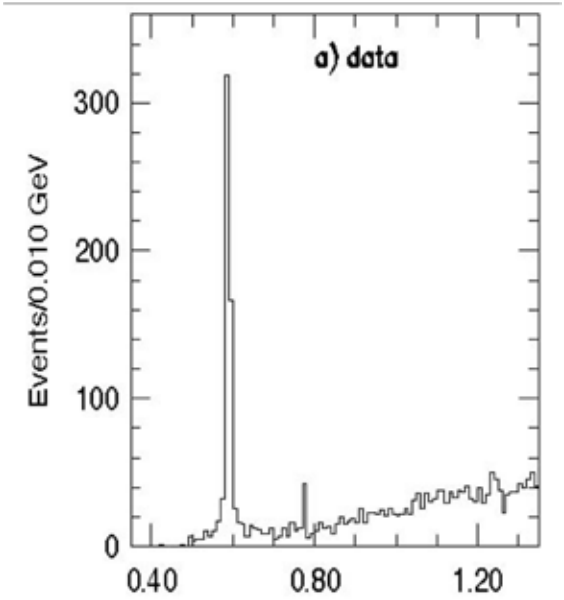

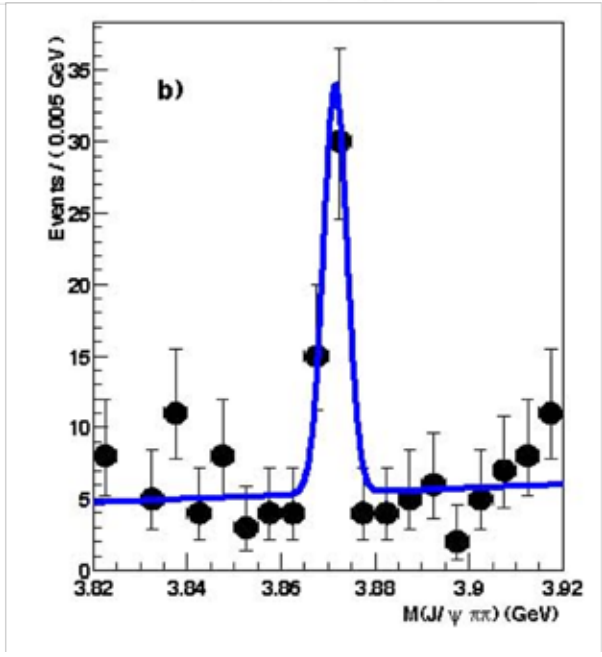

V.2 Open Flavor Production in e^+e^- Collisions

- When a pair of produced heavy quarks $Q\bar{Q}$ form a pair of heavy flavored hadrons, we call this open flavor production
- For $c\bar{c}$ production the charm threshold is at $s^{1/2}=2m_{D0}=3.73$ GeV that is slightly below ψ" having a mass of $M_\psi=3.77$ GeV
- For $b\bar{b}$ production the bottom threshold is at $s^{1/2}=2m_{B0}=10.56$ GeV that is slightly below the $\Upsilon(4S)$ having a mass of $M_\Upsilon=10.58$ GeV
- The simplest sign of open $Q\bar{Q}$ production is a step in the ratio $R=\sigma_{had}/\sigma_{\mu\mu}$

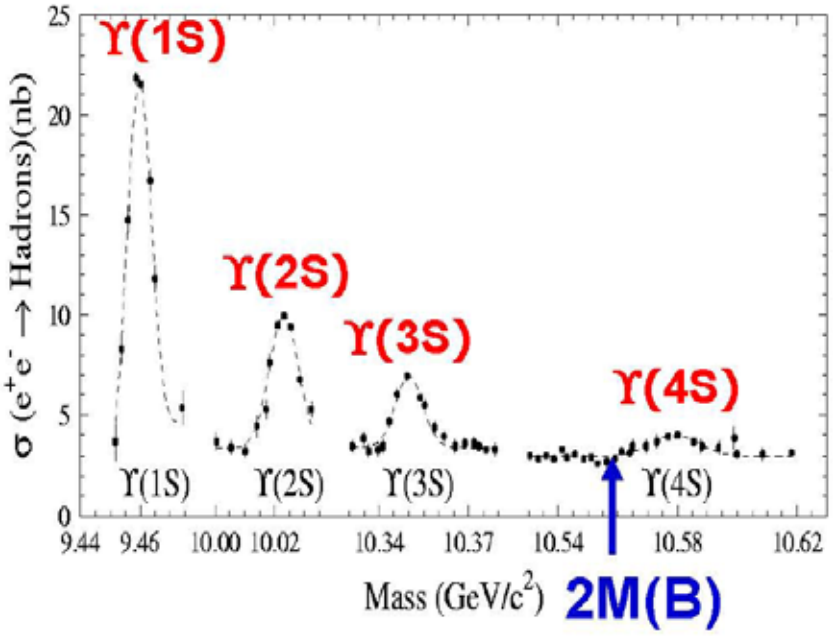

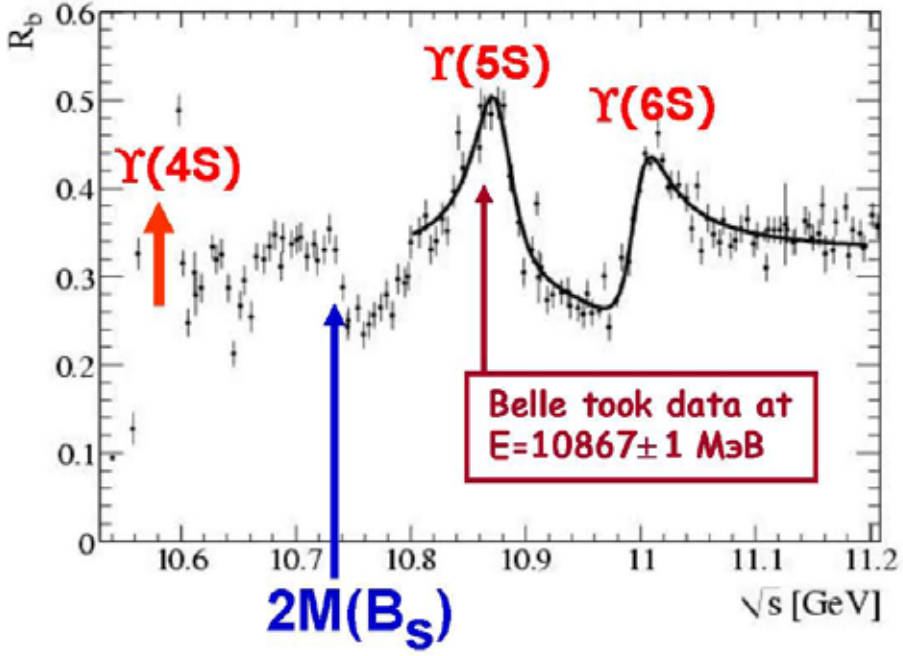

V.3 Quarkonia in Hadroproduction

- Hadroproduction of quarkonium states played an important role for the discovery of $c\bar{c}$ and $b\bar{b}$ bound states
- Unlike e^+e^- collisions, hadron-hadron collisions can produce many quarkonium states directly through subprocesses such as $gg \to (\eta, \chi_0, \chi_2)$, $gg \to \psi g$, $q\bar{q} \to \psi$
- By crossing, these subprocesses are directly related to decay processes $(\eta, \chi_0, \chi_2) \to gg$, $\psi \to ggg$, $\psi \to q\bar{q}$
- The production cross sections are fully determined by the decay width

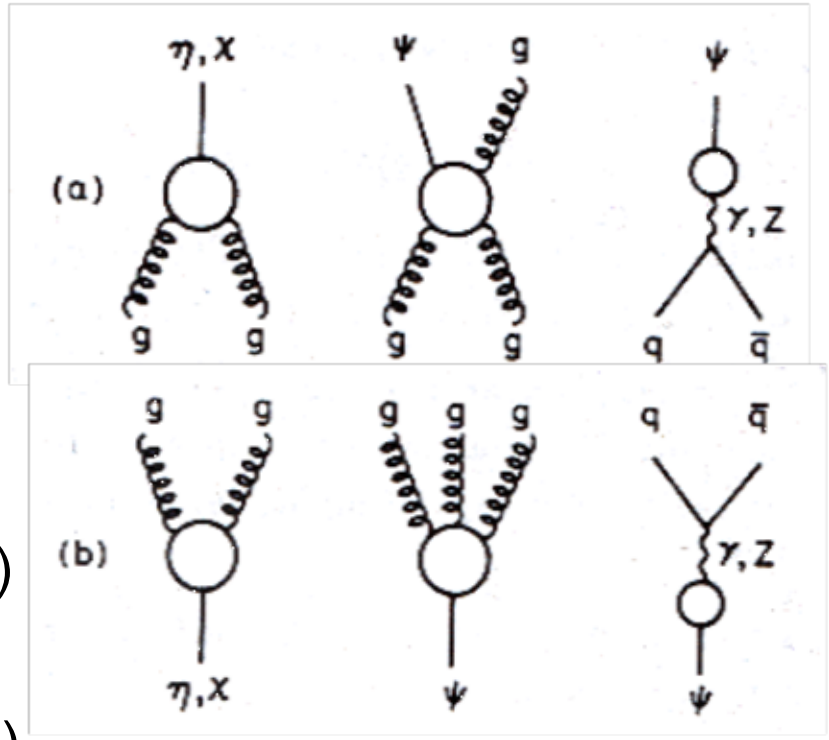

$$\Gamma(\eta_q \to gg) = \frac{8}{3}\alpha_s^2 \frac{|R_s(0)|^2}{m_{\eta_q}^2} \qquad (5.19)$$

$$\Gamma(\chi_0 \to gg) = 96\alpha_s^2 \frac{|R'_P(0)|^2}{m_{\chi_0}^4} \qquad (5.20)$$

$$\Gamma(\chi_2 \to gg) = \frac{128}{5}\alpha_s^2 \frac{|R'_P(0)|^2}{m_{\chi_2}^4} \qquad (5.21)$$

$R_S(0)$ is radial wave function at origin

$R'_P(0)$ is derivative of radial wave function at origin

V.3.1 $(Q\bar{Q})$ in Hadroproduction: Decay Widths

$$\Gamma(\psi \to ggg) = 40\frac{(\pi^2-9)}{81\pi}\alpha_s^3\frac{|R_S(0)|^2}{m_\psi^2} \quad \& \quad \Gamma(\psi \to q\bar{q}) = 12\alpha^2 e_Q^2 e_q^2\frac{|R_S(0)|^2}{m_\psi^2} \tag{5.22}$$ (5.23)

- $R_S(0)$ is the *S*-wave $(Q\bar{Q})$ radial wave function, $R_P(0)$ is the derivative of *P*-wave $(Q\bar{Q})$ radial wave function, α_s is evaluated at the $Q\bar{Q}$ mass scale, e_Q, e_q are electric charges of the heavy, light quarks

- $R(0)$ is related to the total wave function at the origin $\psi(0)$ by

$$|R(0)|^2 = 4\pi|\psi(0)|^2 \tag{5.24}$$

- The cross section for $gg \to \mathcal{O}$, a generic quarkonium state of spin J and mass m_0, is given by

$$\hat{\sigma}(gg \to \mathcal{O}) = \frac{(2J+1)\pi^2}{8m_{\mathcal{O}}^3}\Gamma(\mathcal{O} \to gg)\delta(1-\frac{\hat{s}}{m_{\mathcal{O}}^2}) \tag{5.25}$$

- The hat indicates the quark subprocess, $\hat{s}$ is CM energy squared

- Yang's theorem states that 2 massless spin-1 particles cannot have angular momentum J=1 for a state symmetric in space and spin variables

- Thus, considering Bose statistics and recalling that a color-singlet state of 2 gluons is symmetric in their color variables, forbids $gg \to \psi$

V.3.2 ($Q\bar{Q}$) in Hadroproduction: Cross Section

- So the lowest-order gg subprocess is $gg \to \psi g$, where a bleaching g comes off color in the final state
- The cross section is

$$\hat{\sigma}(gg \to \psi g) = \frac{9\pi^2}{8m_\psi^3(\pi^2 - 9)} \Gamma(\psi \to ggg) I\left(\frac{\hat{s}}{m_\psi^2}\right) \qquad (5.26)$$

where

$$I(x) = \frac{2}{x^2}\left[\frac{x+1}{x-1} - \frac{2x\ln x}{(x-1)^2}\right] + \frac{2(x-1)}{x(x+1)^2} + \frac{4\ln x}{\hat{s}(x+1)} \qquad (5.27)$$

- Note that $I(x)$ is not singular at x=1, $I(1)$=0
- $^3S_1$ states can be produced also by $q\bar{q}$ fusion, the inverse of $\psi \to q\bar{q}$
- The cross section for this process is

$$\hat{\sigma}(q\bar{q} \to \mathcal{O}) = \frac{4\pi^2}{9m_\mathcal{O}^2}(2J+1)\Gamma(\mathcal{O} \to q\bar{q})\delta\left(1 - \frac{\hat{s}}{m_\mathcal{O}^2}\right) \qquad (5.28)$$

- The production of quarkonium states is dominated by gg fusion
- η_c is the most-strongly produced state

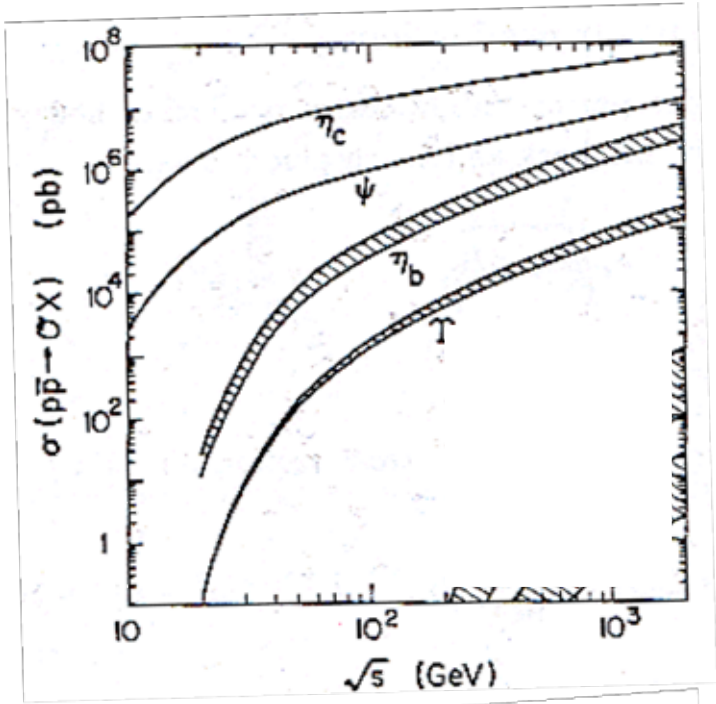

Fig. 10.17. Predicted quarkonium production cross sections in $p\bar{p}$ (or pp) collisions, resulting from $gg \to \mathcal{O}$ subprocesses with enhancement $K = 2$, using Duke-Owens distributions. $\chi_J \to \psi\gamma$ decays are included. Shaded areas represent ranges of uncertainty from potential models. $m_t = 40$ GeV is assumed here.

V.3.3 ($Q\bar{Q}$) Production via $q\bar{q}$ Annihilation

- However, the ψ & Υ states can be identified in $\ell^+\ell^-$ mass distributions while for η_Q states no simple signature exists
- Lowest-order parton subprocesses for production of heavy $Q\bar{Q}$ pairs are $q\bar{q}$ production and gg fusion
- Differential cross section for $q\bar{q}$ fusion

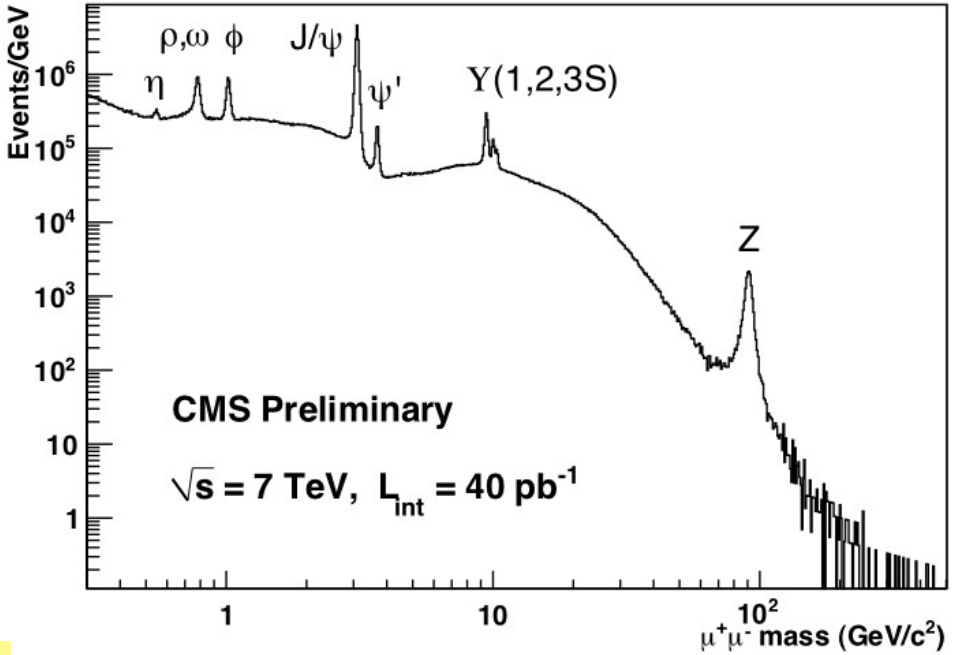

$$\frac{d\hat{\sigma}(q\bar{q}\to Q\bar{Q})}{d\hat{t}} = \frac{4\pi^2}{9\hat{s}^4}\alpha_s^2\left[\left(m^2-\hat{t}\right)^2+\left(m^2-\hat{u}\right)^2+2m^2\hat{s}\right] \quad (5.29)$$

where $\hat{s}=(q+\bar{q})^2$,

$\hat{t}=(q-Q)^2$, $\hat{u}=(q-\bar{Q})^2$

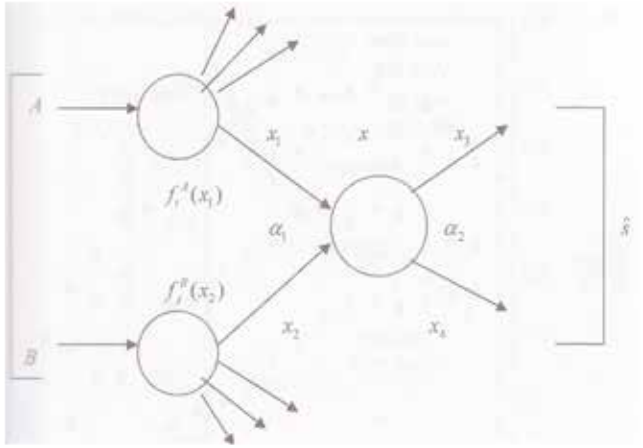

, $q\bar{q}\to Q\bar{Q}$ $gg\to Q\bar{Q}$

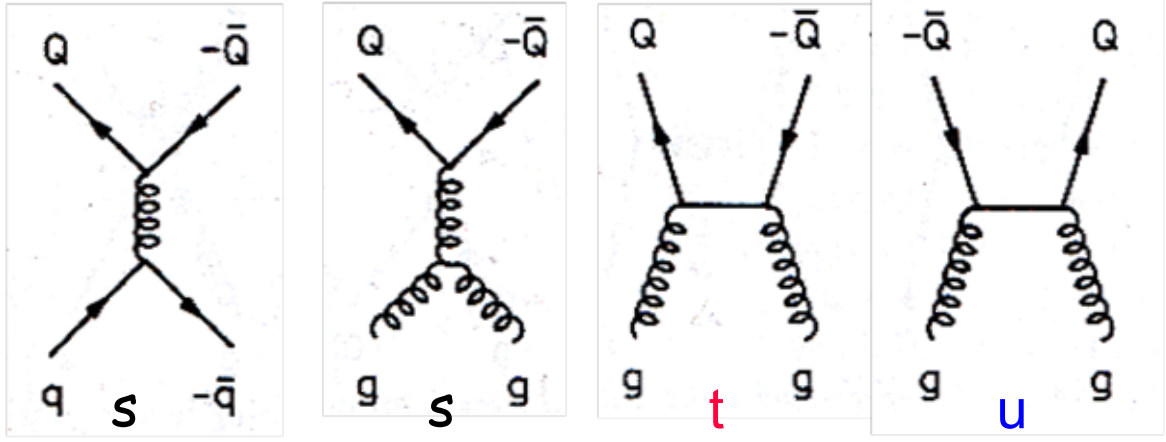

V.3.4 ($Q\bar{Q}$) Production via gg Fusion

- The differential cross section for *gg* fusion is

$$\frac{d\hat{\sigma}(g_1g_2 \to Q\bar{Q})}{d\hat{t}} = \frac{\pi}{8\hat{s}^2}\alpha_s^2\left[\frac{6\left(m^2-\hat{t}\right)\left(m^2-\hat{u}\right)}{\hat{s}^2} - \frac{m^2\left(\hat{s}-4m^2\right)}{3\left(m^2-\hat{t}\right)\left(m^2-\hat{u}\right)}\right] \leftarrow \text{s} \qquad (5.30)$$

$$+\frac{4}{3}\frac{\left(m^2-\hat{t}\right)\left(m^2-\hat{u}\right)-2m^2\left(m^2+\hat{t}\right)}{\left(m^2-\hat{t}\right)^2} - 3\frac{\left(m^2-\hat{t}\right)\left(m^2-\hat{u}\right)+m^2\left(\hat{u}-\hat{t}\right)}{\hat{s}\left(m^2-\hat{t}\right)} \leftarrow \text{t}$$

$$+\frac{4}{3}\frac{\left(m^2-\hat{t}\right)\left(m^2-\hat{u}\right)-2m^2\left(m^2+\hat{u}\right)}{\left(m^2-\hat{u}\right)^2} - 3\frac{\left(m^2-\hat{t}\right)\left(m^2-\hat{u}\right)+m^2\left(\hat{t}-\hat{u}\right)}{\hat{s}\left(m^2-\hat{u}\right)}\Bigg] \leftarrow \text{u}$$

symmetry

where $\hat{s}=(g_1+g_2)^2$, $\hat{t}=(g_1-Q)^2$, $\hat{u}=(g_1-\bar{Q})^2$

- Note, that the $\hat{t}^{-2}$ and $\hat{u}^{-2}$ singularities of $gg \to qq$ massless quark production have been removed by the presence of $m_Q=m$, since $\hat{t}<0$ and $\hat{u}<0$ due to kinematics
- The running coupling constant $\alpha_s(Q^2)$ is evaluated at appropriate scale, usually $Q^2=p^2_T$, $\hat{s}/4$ or $\hat{s}$
- For the latter choice $\alpha_s(Q^2)$ is finite at small p_T

V.4 Open Flavor in Hadroproduction

- There are also flavor excitation processes in which a heavy quark is scattered out of the sea in one of the incident hadrons

$qQ \to qQ$ $\quad$ $gQ \to gQ$

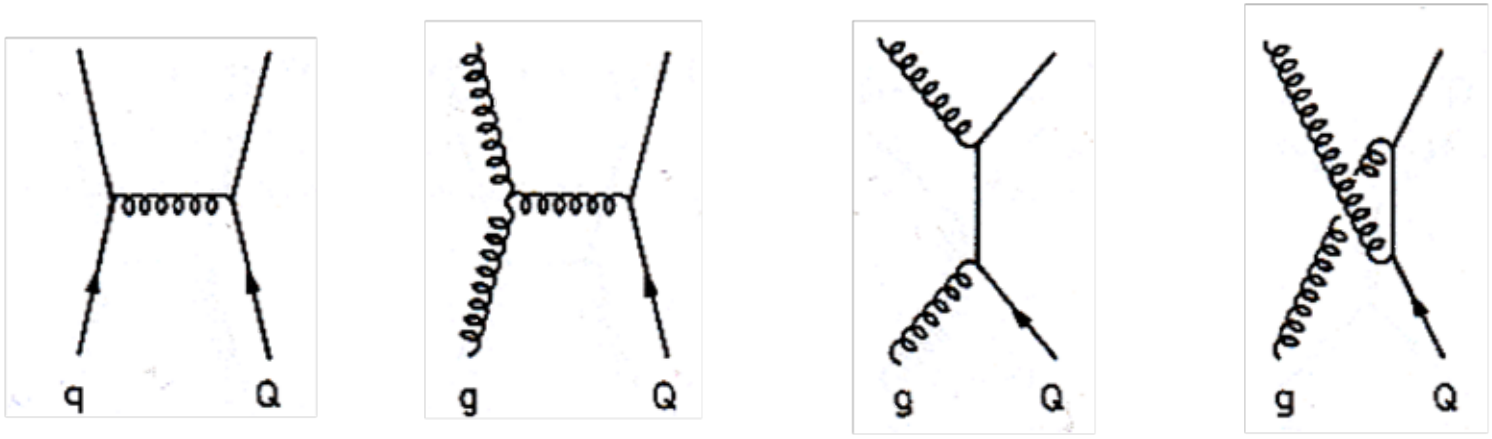

Fig. 10.20. Flavor-excitation subprocesses producing heavy quarks Q (and $\bar{Q}$).

- The corresponding cross sections are

$$\frac{d\hat{\sigma}(qQ \to q'Q')}{d\hat{t}} = \frac{4\pi}{9\hat{s}^2}\alpha_s^2\left[\frac{\left(m^2-\hat{u}\right)^2+\left(\hat{s}-m^2\right)^2-m^2\hat{t}}{\hat{t}^2}\right] \qquad (5.31)$$

where $\hat{s}=(q+Q)^2$, $\hat{t}=(q-q')^2$, $\hat{u}=(q-Q')^2$

V.4.1 Q Production via Gluons

$$\frac{d\hat{\sigma}(gQ\to g'Q')}{d\hat{t}}=\frac{\pi}{\hat{s}^2}\alpha_s^2\left[\frac{2\left(\hat{s}-m^2\right)\left(m^2-\hat{u}\right)}{\hat{t}^2}-\frac{m^2\left(4m^2-\hat{t}\right)}{9\left(\hat{s}-m^2\right)\left(m^2-\hat{u}\right)}\right]\leftarrow \boxed{t}$$

$$\boxed{s}\rightarrow +\frac{4}{9}\frac{\left(\hat{s}-m^2\right)\left(m^2-\hat{u}\right)+2m^2\left(\hat{s}+m^2\right)}{\left(\hat{s}-m^2\right)^2}+\frac{\left(\hat{s}-m^2\right)\left(m^2-\hat{u}\right)+m^2\left(\hat{s}-\hat{u}\right)}{\hat{t}\left(\hat{s}-m^2\right)}$$

$$+\frac{4}{9}\frac{\left(\hat{s}-m^2\right)\left(m^2-\hat{u}\right)+2m^2\left(m^2+\hat{u}\right)}{\left(m^2-\hat{u}\right)^2}+\frac{\left(\hat{s}-m^2\right)\left(m^2-\hat{u}\right)+m^2\left(\hat{u}-\hat{s}\right)}{\hat{t}\left(\hat{u}-m^2\right)}\leftarrow \boxed{u}$$

(5.32)

where $\hat{s}=(g+Q)^2$, $\hat{t}=(g-g')^2$, $\hat{u}=(g-Q')^2$

$s \leftrightarrow u$ symmetry

➔ obtain from eq 5.30 by crossing relation $t \leftrightarrow s$, & factor (-1)

❒ These flavor excitations subprocesses present some difficulties, when we try to calculate realistic final states from them

i) It is not possible to arrange realistic kinematics to allow both the struck quark Q & its partner $\bar{Q}$ to come on-shell in a single collision where $\bar{Q}$ is unseen and unspecified

ii) It is unsatisfactory not to know what happened to Q, so we may want to include its decays products in the final state

V.4.2 $Q\bar{Q}g$ and $Q\bar{Q}q$ Production

- iii) Subprocess cross sections have soft & collinear divergences at $\hat{t}=0$, where the exchange gluon comes into its mass shell seeming to require an arbitrary cut-off

- Difficulties (i) & (ii) resemble problems of exciting heavy sea quarks in EW lepton scattering

- The solution is to go to higher-order QCD, where explicit $g \to Q\bar{Q}$ vertices provide a dynamical model of the $Q\bar{Q}$ sea

- The $2 \to 3$ parton subprocesses that produce $Q\bar{Q}$ pairs are

$q\bar{q} \to Q\bar{Q}\, g$ $\quad$ $gq(\bar{q}) \to Q\bar{Q}\, q(\bar{q})$ $\quad$ $gg \to Q\bar{Q}\, g$

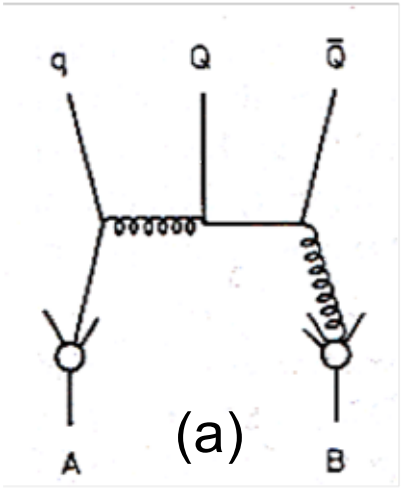

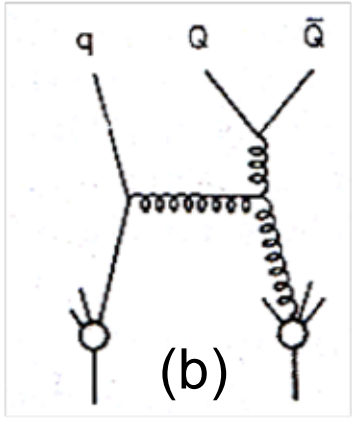

Fig. 10.21. Examples of $2 \to 3$ parton processes producing $Q\bar{Q}$ heavy quark pairs in the collision of hadrons A and B: (a) flavor excitation of the sea, (b) gluon fragmentation.

V.4.2 $Q\bar{Q}g$ and $Q\bar{Q}q$ Production

- Lowest-order contributions are $\mathcal{O}(\alpha_s^3)$ tree graphs yielding rather lengthy formula (see Nuc. Phys. B282, 643 1987)

- The above graphs show some interesting feature

iv) They show flavor excitation $qQ \to qQ$ scattering from a $Q\bar{Q}$ pair explicitly generated by a gluon (solves problems i & ii), since heavy quark kinematics are specifically put in and we exactly know what happened to the spectator Q

v) they have soft and collinear divergences when $p_T(Q\bar{Q}) \to 0$ and the momentum of exchanged gluon goes on-shell ➔ problem iii

- when this, however, happens, we can see that the on-shell gluon is simply part of an empirical parton distribution in hadron A, so this configuration is already included in gluon fusion cross section $gg \to Q\bar{Q}$
- Thus, a major part of the flavor excitation is already included in gg, $q\bar{q} \to Q\bar{Q}$ calculation ➔ it would be double counting if it were included separately ➔ the cut-off should be at the scale of evolution of the parton distribution

V.4.2 $Q\bar{Q}g$ and $Q\bar{Q}q$ Production

- vi) Figure b illustrates gluon fragmentation as a source of $Q\bar{Q}$ pairs
  - The hard contributions originate from highly virtual gluons, while soft fragmentation is not expected to produce $Q\bar{Q}$ As shown here, they appear explicitly in order $\mathcal{O}(\alpha_s{}^3)$ (higher orders can be calculated by MC shower techniques)
  - Gluon fragmentation is expected to be the major source of $c\bar{c}$ & $b\bar{b}$ production at the LHC

- Lets compare gluon fragmentation to gluon fusion

$$\frac{\sigma(gg \to Q\bar{Q}g)}{\sigma(gg \to Q\bar{Q})} \simeq \frac{\sigma(gg \to gg)}{\sigma(gg \to Q\bar{Q})} \frac{\alpha_s(4m_Q^2)}{3\pi} \ln\left(\frac{\hat{s}}{4m_Q^2}\right) \qquad (5.33)$$

- If $\hat{s} \gg 4m^2_Q$, gluon fragmentation dominates over gluon fusion as $Q\bar{Q}$ source

- To avoid double counting, the strategy is to focus on $2\to2$ and $2\to3$ channels for $Q\bar{Q}$ production

V.4.2 $Q\bar{Q}g$ and $Q\bar{Q}q$ Production

- The total cross section is approximately given by the $2\rightarrow2$ subprocesses $q\bar{q}\rightarrow Q\bar{Q}$ and $gg\rightarrow Q\bar{Q}$, evolving them up to the appropriate scale $Q^2 = p^2_T + m^2_Q$ or $\hat{s}/4$
- Major contributions from flavor excitations and $2\rightarrow3$ channels arise when the exchanged gluon approaches the mass shell that are already included in $qQ\rightarrow qQ$ and $gQ\rightarrow gQ$ diagrams
- Thus, the diagram of $2\rightarrow3$ channels in a) and b) do not give large additional contributions
- In effect, we assume that $Q\bar{Q}$ was produced by 2 gluons, one from each hadron or else from one gluon where 2 parents from this gluon came from different hadrons
- This includes all $\mathcal{O}(\alpha_s^3)$ quark-excitation-type processes and some of the gluon fragmentation, except for gluons in initial-state or final-state showers

V.4.3 $Q\bar{Q}$ via EW Production

- Furthermore, EW channels need to be added: $q\bar{q}' \rightarrow W^{\pm} \rightarrow Q\bar{Q}'$, $q\bar{q} \rightarrow \gamma \rightarrow Q\bar{Q}$ and $q\bar{q} \rightarrow Z^0 \rightarrow Q\bar{Q}$

- These contributions are very small compared to QCD

- The EW calculations can be normalized to $W \rightarrow e\nu$ and $Z \rightarrow e^+e^-$ data

- Using parton distributions by the D0 experiment typical predictions at $s^{1/2}$=630 GeV and $s^{1/2}$=2 TeV for $Q^2 = \hat{s}/4$, Λ=0.2 GeV, n_f=5, first-order α_s corrections and but without other non-LLA corrections

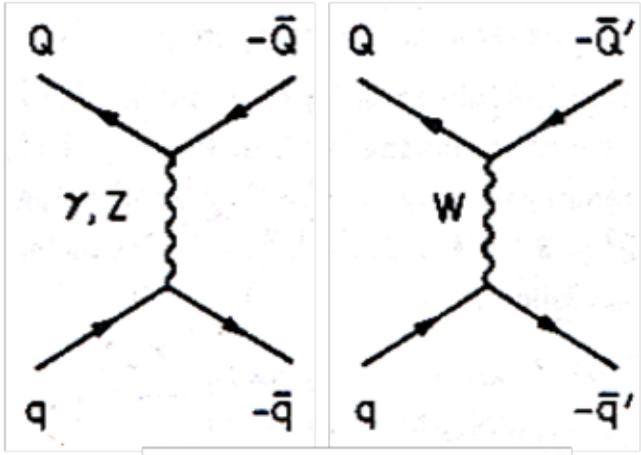

Fig. 10.22. Electroweak contributions to heavy quark hadroproduction.

cross section	$s^{1/2}$=630 GeV	$s^{1/2}$=2 TeV
$\sigma(\text{QCD} \rightarrow c\bar{c})$	140 μb	300 μb
$\sigma(\text{QCD} \rightarrow b\bar{b})$	6 μb	25 μb
$\sigma(\text{QCD} \rightarrow t\bar{t})$	<0.6 μb	<10 μb

V.4.4 $Q\bar{Q}$ Production: Recombination

cross section	$s^{1/2}$=630 GeV	$s^{1/2}$=2 TeV
$\sigma(Z\to c\bar{c})$	0.2 nb	0.8 nb
$\sigma(Z\to b\bar{b})$	0.3 nb	1.0 nb
$\sigma(W\to c\bar{s})$	1.7 nb	5.8 nb

- Besides perturbative QCD & EW production 2 other processes contribute

a) recombination: a heavy quark may be picked up by one or more valence quarks & form a fast baryon qqQ or meson $q\bar{Q}$ ➔ fast flavored hadrons (small effect on total cross section)

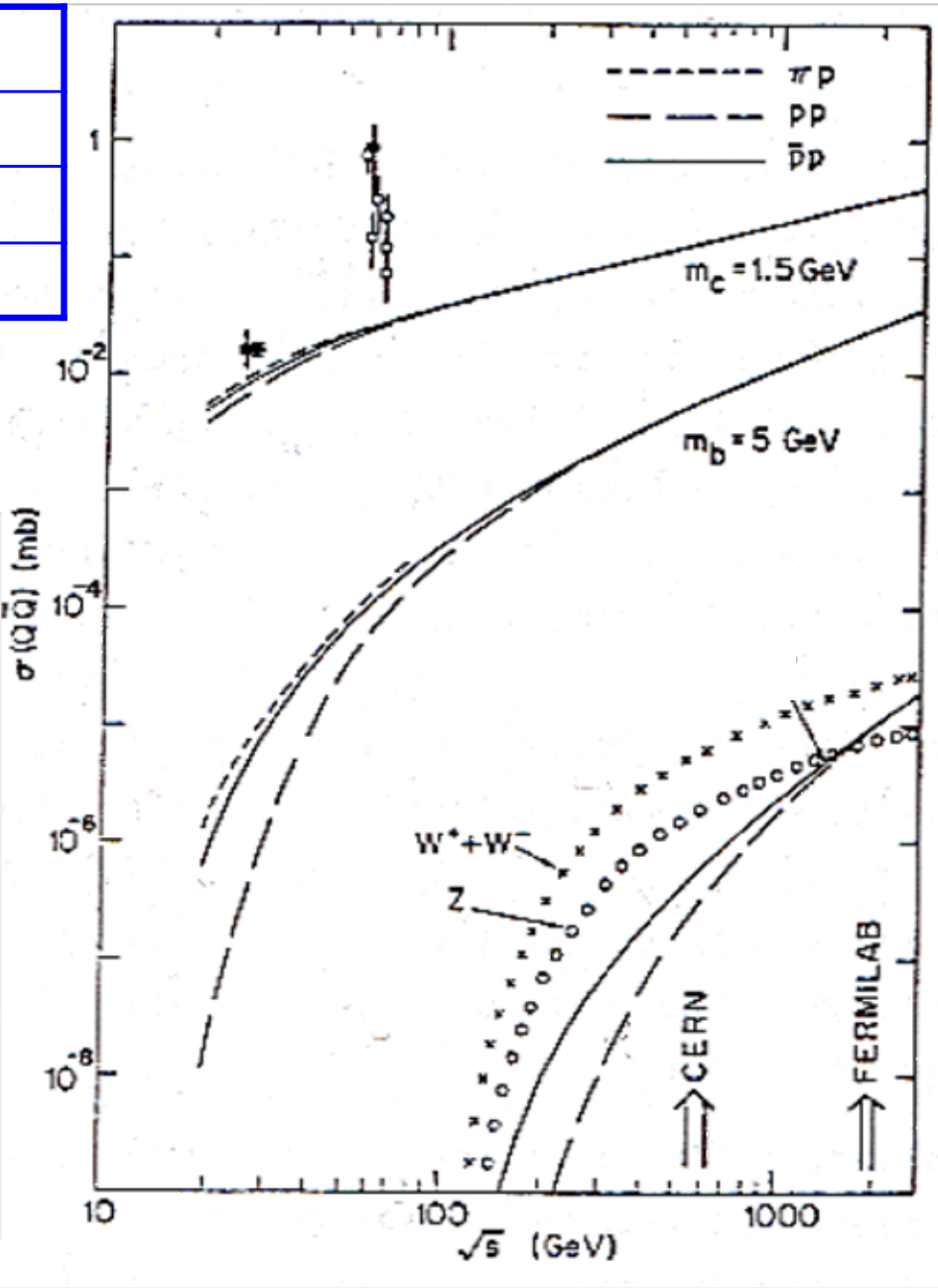

Fig. 10.23. Calculations of heavy flavor production based on $2 \to 2$ subprocesses for πp, pp and $p\bar{p}$ collisions, compared to a few selected data points. Data at $\sqrt{s} \simeq 60$ GeV are for pp. Data at $\sqrt{s} \simeq 25$ GeV are for πp (star) and pp (circle). The cross sections for $W^{\pm}$ and Z^0 production are also shown.

V.4 V.4.5 $Q\bar{Q}$ Production: Diffraction

b) diffraction: the incident p is excited by vacuum exchange to a high mass N^* with essentially unchanged energy that can decay into Q-flavored hadrons, one of which can be fast

- Both processes cannot be reliably predicted
- They are characterized by low p_T and high x_F ($x_F = p_D^{long}/p_{max}$)

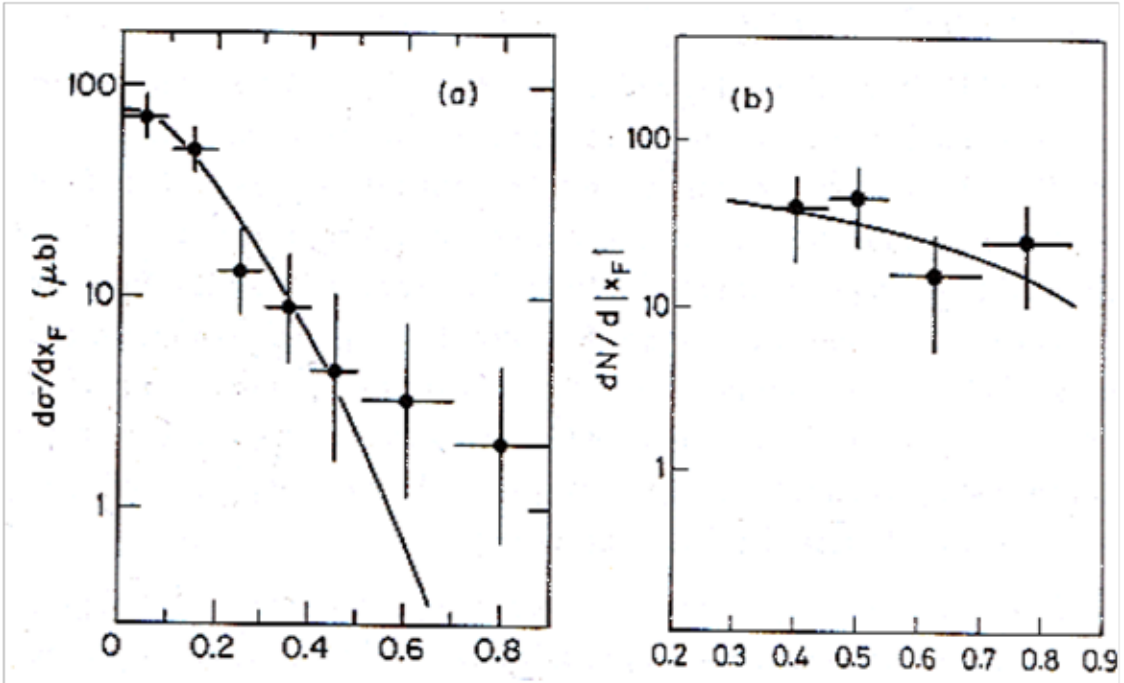

Fig. 10.24. (a) x_F dependence of inclusive $\pi p \to D$ production with $x_F > 0$ at $\sqrt{s} = 26$ GeV (NA27 experiment, Phys. Lett. **161B**, 400 (1985)); the curve is a $2 \to 2$ QCD calculation with δ-function fragmentation, normalized to the data. (b) x_F dependence of inclusive $pp \to \Lambda_c$ production at $\sqrt{s} = 63$ GeV (CERN-Bologna group, Nuovo Cim. **65A**, 408 (1981); the curve is an empirical fit $\sim (1 - |x_F|)^{0.9}$.

- Present data are contradictory: In $\pi p \to DX$ charm production we observe a 20% diffractive component in $d\sigma/dx_F \sim (1-|x_F|)^n$ with n=1-2, while rest agrees with QCD fusion with n=6-8

V.4.5 $Q\bar{Q}$ Production: Open Charm

- Charm production in CDF

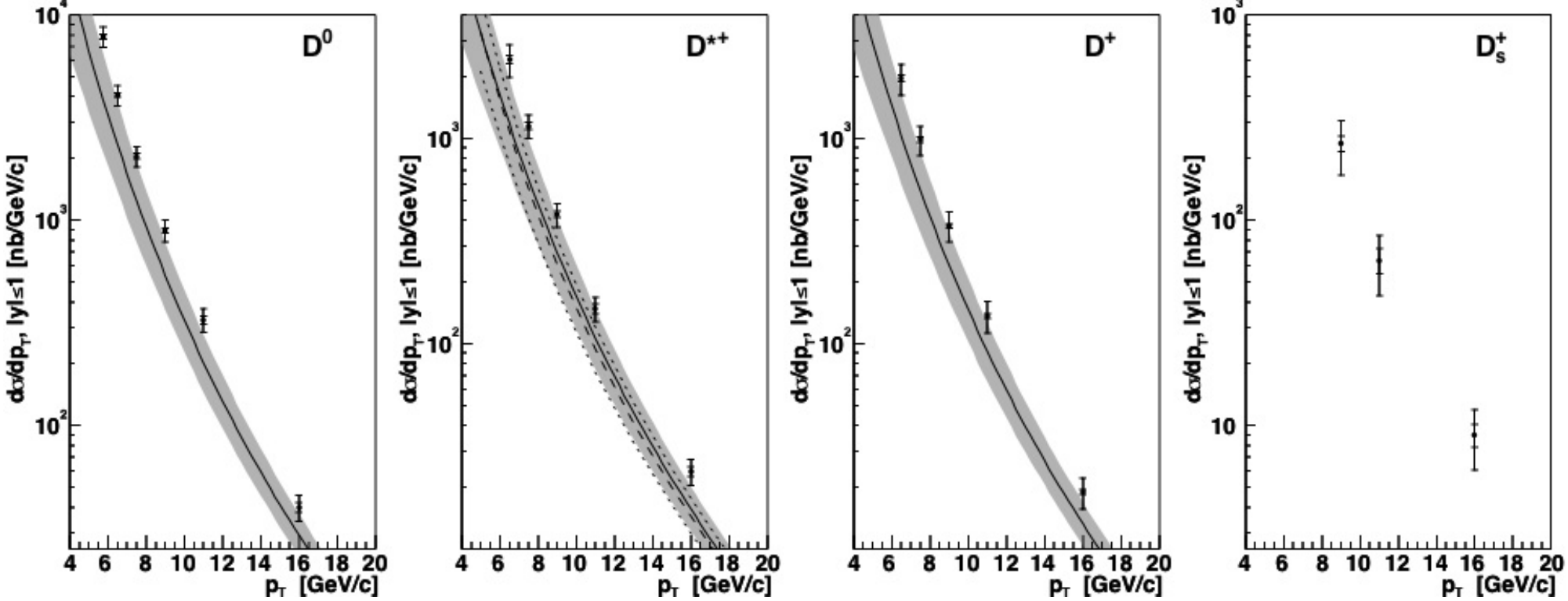

- The observed cross sections are

$$\sigma(D^0)_{p_t>6\ \mathrm{GeV}} = 9.3 \pm 0.1 \pm 1.1\ \mathrm{pb}$$

$$\sigma(D^{*\pm})_{p_t>6\ \mathrm{GeV}} = 5.1 \pm 0.1 \pm 0.8\ \mathrm{pb}$$

$$\sigma(D^{\pm})_{p_t>6\ \mathrm{GeV}} = 4.2 \pm 0.1 \pm 0.7\ \mathrm{pb}$$

(5.34)

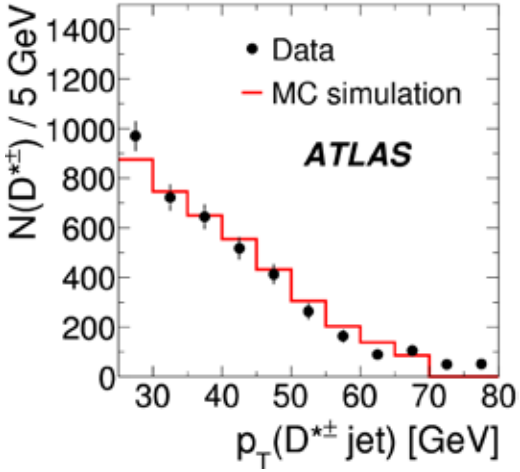

V.4.6 $Q\bar{Q}$ Production: Open Charm and Beauty

- We also see an excess of D mesons that share the valence quark with the incident π, $\pi^+ \rightarrow D^0, D^+$ but not $\pi^+ \rightarrow \bar{D}^0, D^-$
- In contrast, the ISR data for $pp \rightarrow \Lambda^+_c X$ suggest an overwhelming diffractive component but such a strong onset of diffraction over a relatively small change of energy would be surprising (open issue)
- Note that the heavy quarks are tagged by leptons or in a new jet
- Actually, B^0-$\bar{B}^0$ oscillations were discovered that way
- UA1 looked at the ratio of like-sign to unlike-sign leptons

$$\frac{N^{\pm\pm}}{N^{\pm\mp}} = \frac{2\chi(1-\chi)}{\chi^2 + (1-\chi)^2} \qquad \chi = f_d \chi_d + f_s \chi_s \tag{5.35}$$

- χ gives the probability for oscillations $B^0 \rightarrow \bar{B}^0$
- In a sample of 512 $\mu\mu$ events they measured

$$\chi = 0.121 \pm 0.047 \tag{5.36}$$

- Note, though $\chi = x^2/(2x^2+2)$ and x_d has been measured this does not give the sensitivity to extract x_s

V.5 Production of the top Quark

- CDF & D0 discovered the top quark in $p\bar{p} \rightarrow t\bar{t}\,X$ in 1995
- The decay proceeds 100% via $t \rightarrow bW^+$
- Since W bosons decay as $W^+ \rightarrow \ell^+ \nu$ or $q\bar{q}$, we get 3 classes of events: $\ell^+ \ell'^- \nu\bar{\nu}' b\bar{b}$, $\ell\nu q\bar{q}' b\bar{b}$ or $q_1\bar{q}'_1 q_2\bar{q}'_2 b\bar{b}$
  ➔ 2 leptons plus 2 jets, 1 lepton plus 4 jets or 6 jets
- The top was observed first in the $\ell\nu q\bar{q}' b\bar{b}$ decay with a W mass constraint in the lν decay
- CDF reconstructed m_t templates in terms of top mass and jet energy scale (JES) ➔ extract m_t pdfs from multidimensional templates
- Construct W-mass templates as a function of m_t & JES and background templates that are independent of m_t and JES
- Validate technique on independent sample
- CDF and D0 measured mass and other properties in all channels

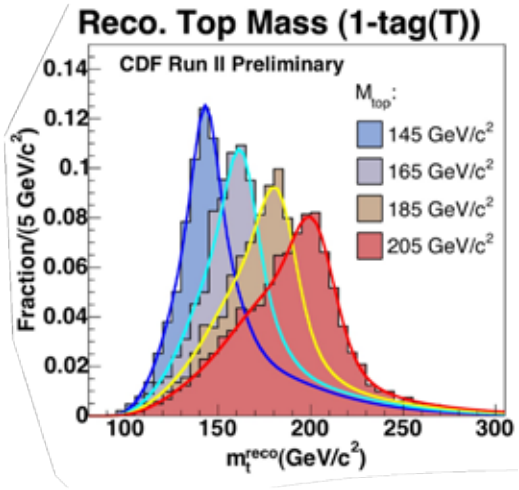

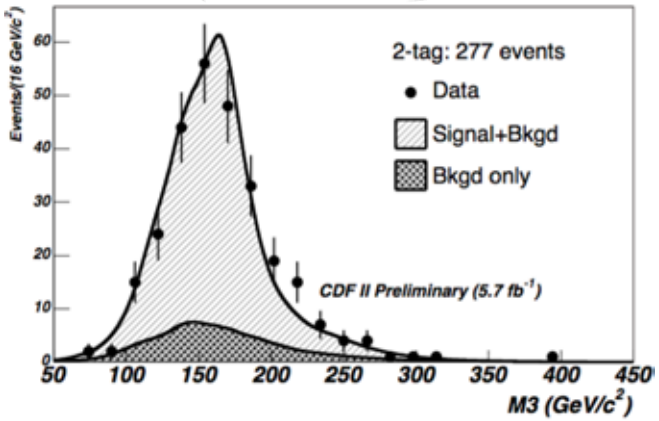

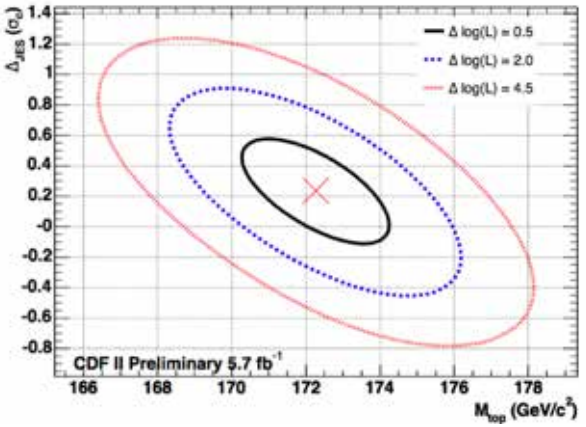

V.5.1 Top Quark at LHC

- ATLAS and CMS have measured the top quark properties
- In the $t\bar{t} \rightarrow b\bar{b}j_1j_2j_3j_4$ analysis ATLAS reconstructs a c^2 based on j_1j_2, j_3j_4 and bj_1j_2 or bj_3j_4 masses producing templates for the 3-jet/2-jet mass ratio: $R_{3/2}$
- Generate $R_{3/2}$ distributions with different masses (template)
- Measure top mass

$$m_{top} = 173.72 \pm 0.55_{stat} \pm 1.01_{sys}\ GeV \qquad (5.36)$$

W mass

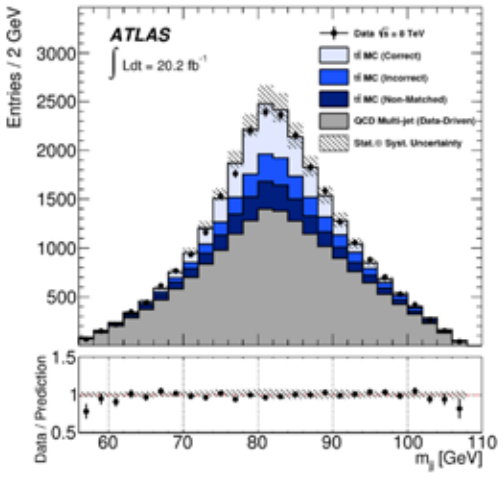

Top mass

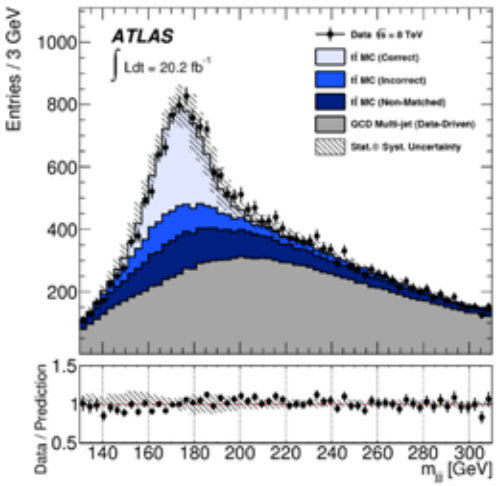

MC $R_{3/2}$ for 172.5 GeV

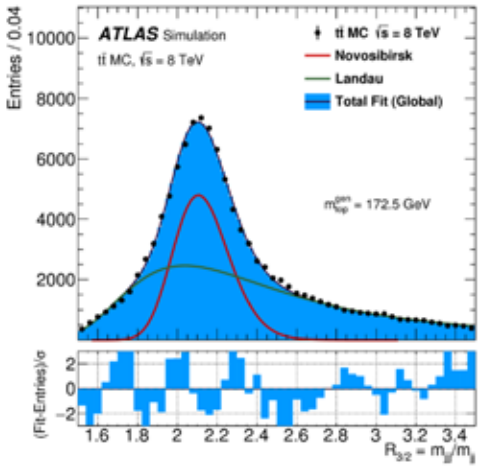

Observed $R_{3/2}$ wrt simulated signal and backgrounds

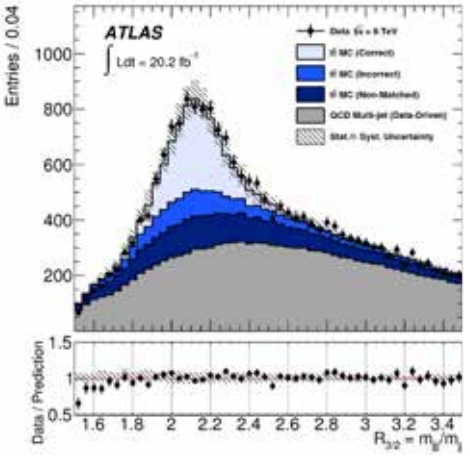

Observed $R_{3/2}$ fit to signal plus background templates

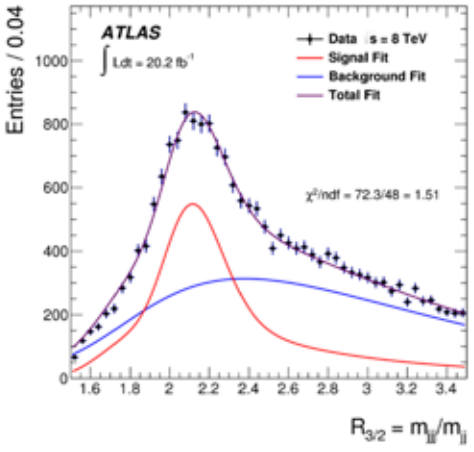

- $R_{3/2}$ distribution generated for different m_t
- Fit signal with Novosibirsk and background Landau functions

V.5.1 Top Quark at LHC

- In the $b\ell\nu$ channel ATLAS measures $m_{top} = 172.99 \pm 0.41_{stat} \pm 0.74_{sys}\ GeV$ (5.37)
- The ATLAS m_t average yields $m_{top} = 172.84 \pm 0.34_{stat} \pm 0.61_{sys}\ GeV$ (5.38)
- In comparison, CMS obtains $m_{top} = 172.44 \pm 0.13_{stat} \pm 0.47_{sys}\ GeV$ (5.39)

- $t\bar{t}$ event observed by ATLAS in the $\ell^+\ell'^-\nu\bar{\nu}b\bar{b}$ channel

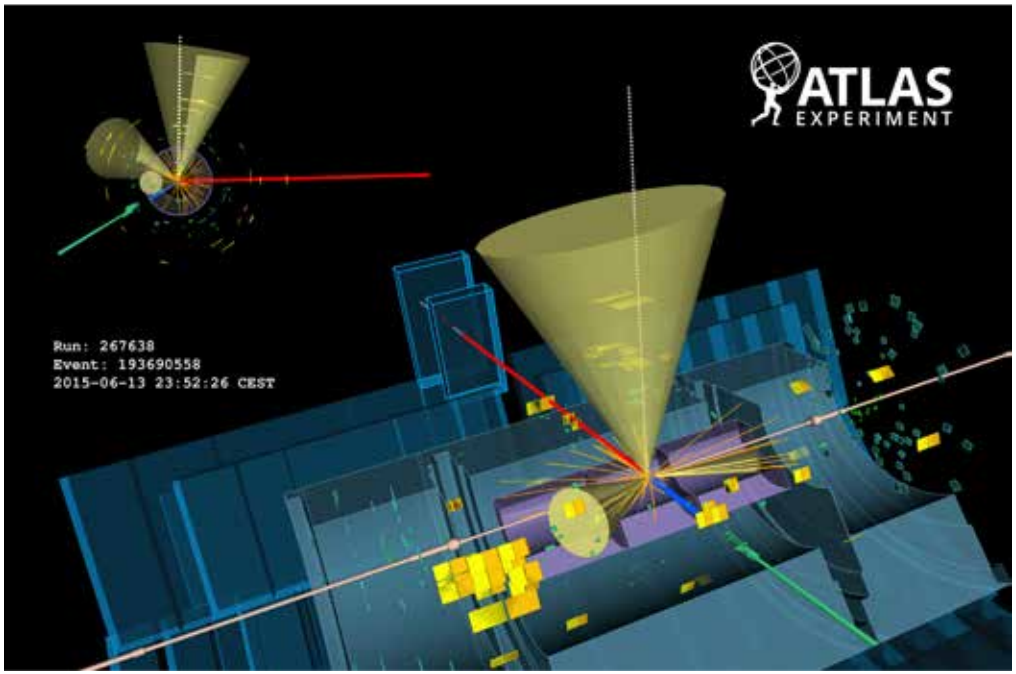

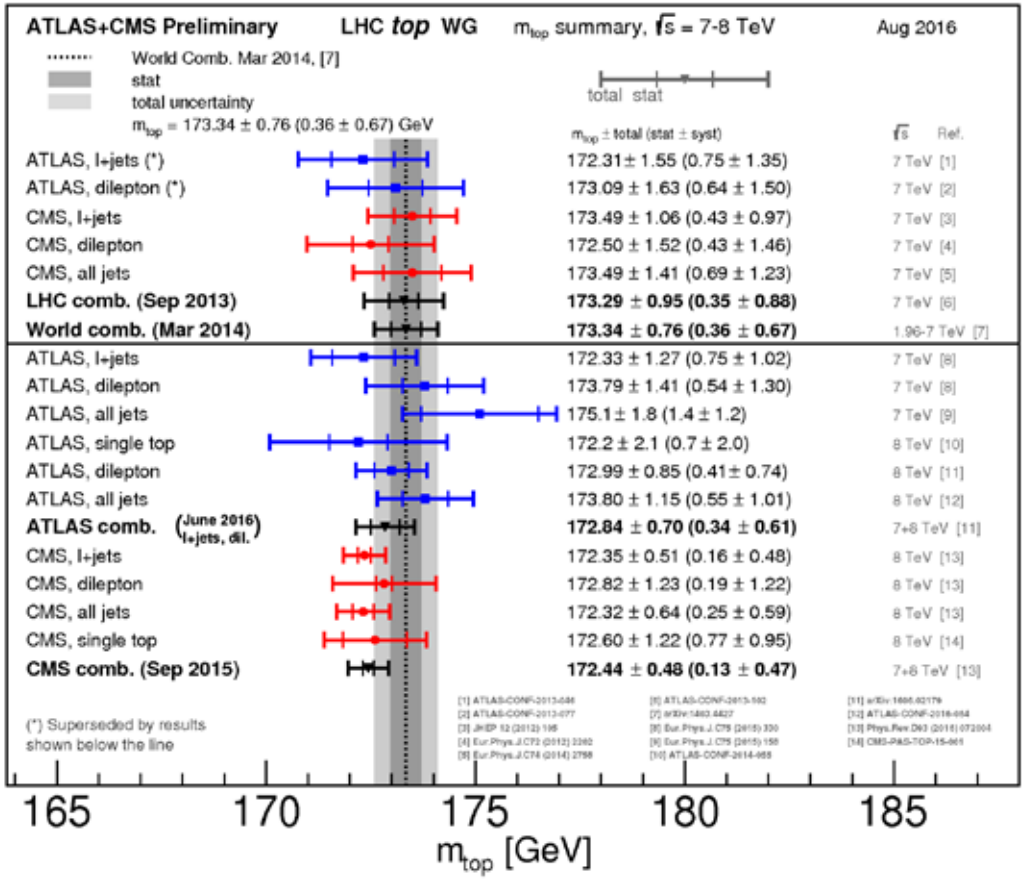

V.5.1 Top Quark at LHC

- Differential cross section as function $p_T(t\bar{t})$ falls rapidly in good agreement with prediction
- Total $t\bar{t}$ cross section agrees well with NNLL prediction for all measurements
- Furthermore, NNLL prediction describes well $pp \rightarrow t\bar{t}X$ cross section measurements at LHC and $p\bar{p} \rightarrow t\bar{t}X$ cross section measurements at Tevatron

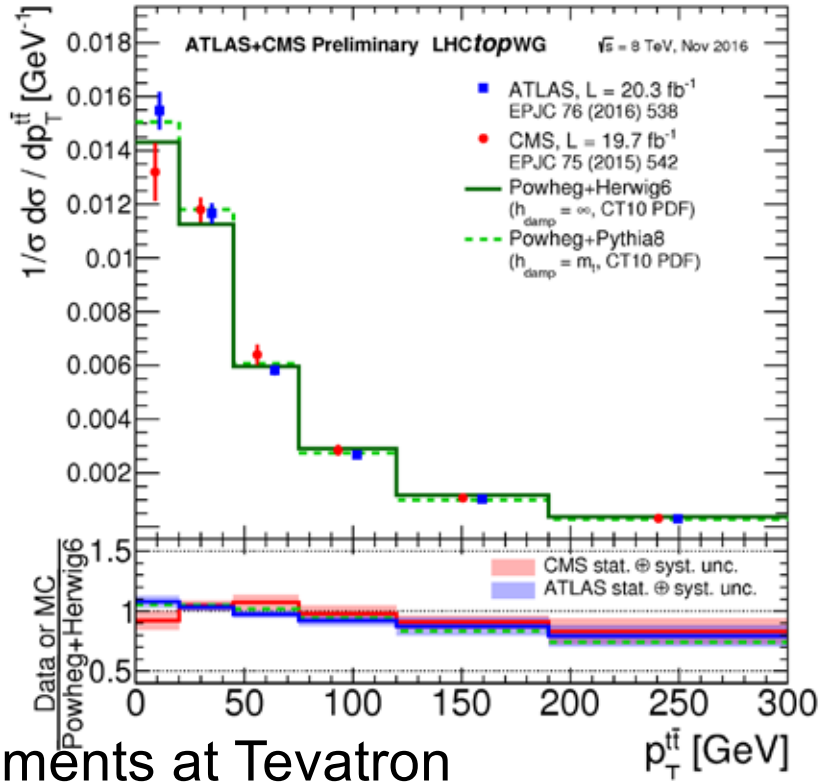

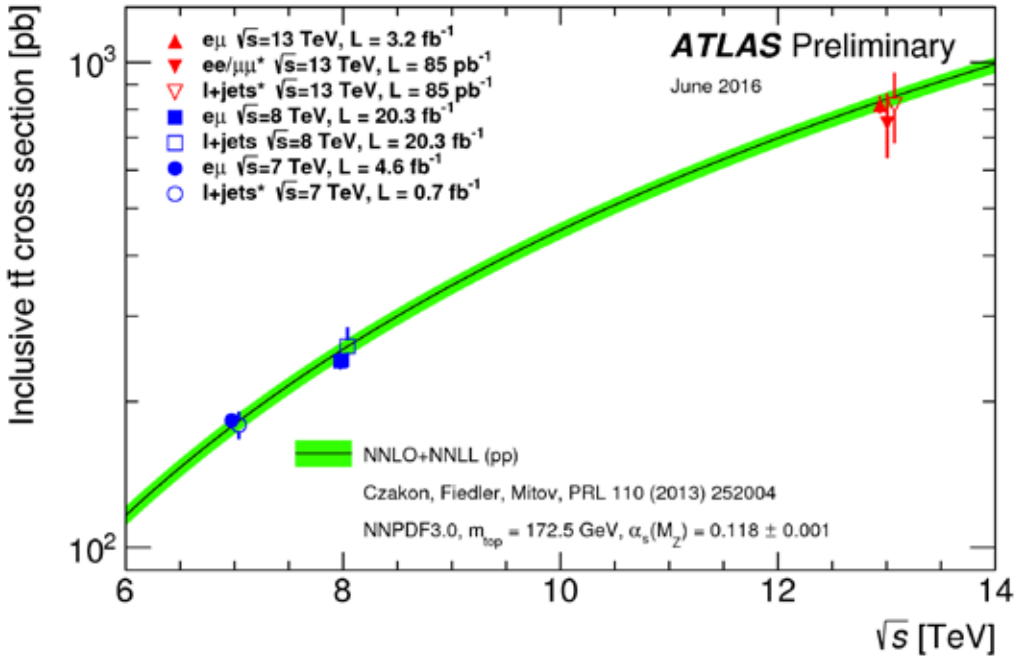

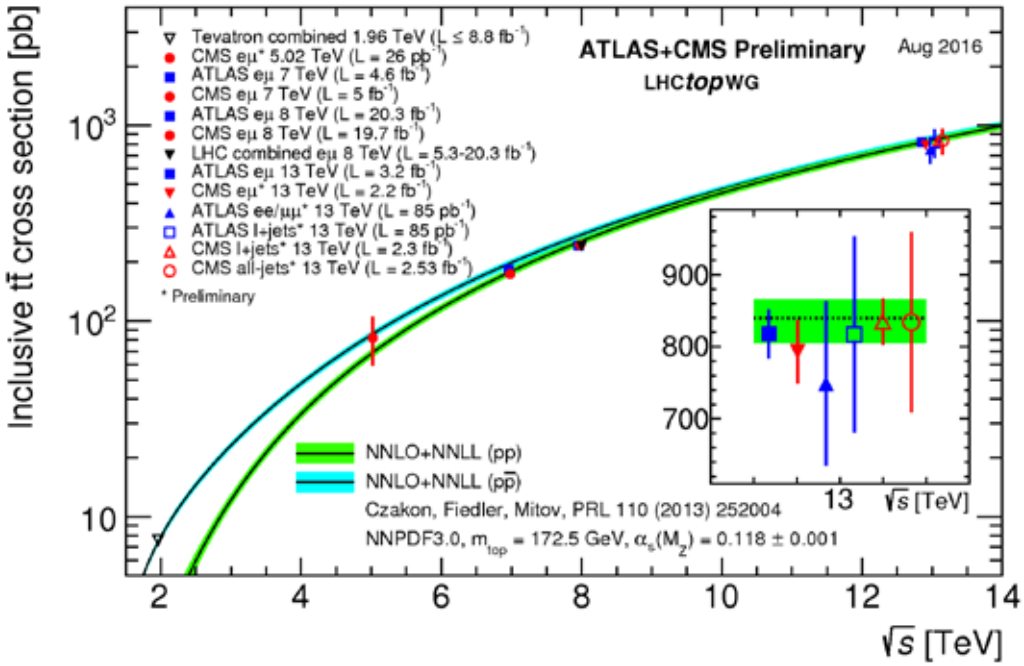

V.5.2 $t\bar{t}\,W$ and $t\bar{t}\,Z$ Production

- ATLAS measured $t\bar{t}\,W$ and $t\bar{t}\,Z$ Production at 8 TeV using 4 signal decay topologies for each vector boson and 5 control regions
- Use neural network to separate $t\bar{t}\,W$ & $t\bar{t}\,Z$ signal from backgrounds (7 inputs)
- See significant signal yields & measure cross sections consistent with the SM

$$\sigma_{t\bar{t}W} = 369^{+86}_{-79(stat)} \pm 44_{sys}\, fb \text{ (5 s.d.)} \qquad (5.40)$$

$$\sigma_{t\bar{t}Z} = 176^{+52}_{-48(stat)} \pm 24_{sys}\, fb \text{ (4.2 s.d.)} \qquad (5.41)$$

- CMS has similar results

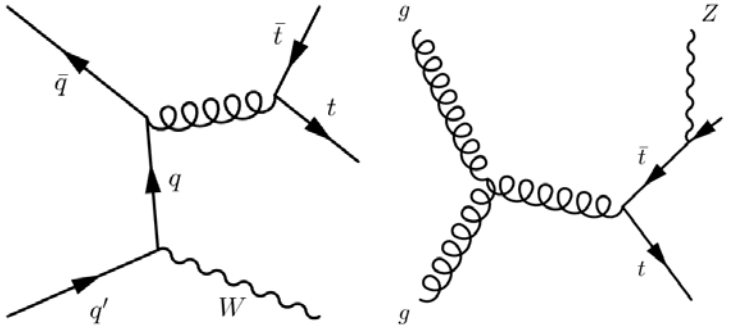

Process	$t\bar{t}$ decay	Boson decay	Channel	$Z \to \ell^+\ell^-$
$t\bar{t}W^{\pm}$	$(\ell^{\pm}\nu b)(q\bar{q}b)$	$\ell^{\mp}\nu$	OS dilepton	no
	$(\ell^{\pm}\nu b)(\ell^{\mp}\nu b)$	$q\bar{q}$	OS dilepton	no
	$(\ell^{\pm}\nu b)(q\bar{q}b)$	$\ell^{\pm}\nu$	SS dilepton	no
	$(\ell^{\pm}\nu b)(\ell^{\mp}\nu b)$	$\ell^{\pm}\nu$	Trilepton	no
$t\bar{t}Z$	$(\ell^{\pm}\nu b)(\ell^{\mp}\nu b)$	$q\bar{q}$	OS dilepton	no
	$(q\bar{q}b)(q\bar{q}b)$	$\ell^+\ell^-$	OS dilepton	yes
	$(\ell^{\pm}\nu b)(q\bar{q}b)$	$\ell^+\ell^-$	Trilepton	yes
	$(\ell^{\pm}\nu b)(\ell^{\mp}\nu b)$	$\ell^+\ell^-$	Tetralepton	yes

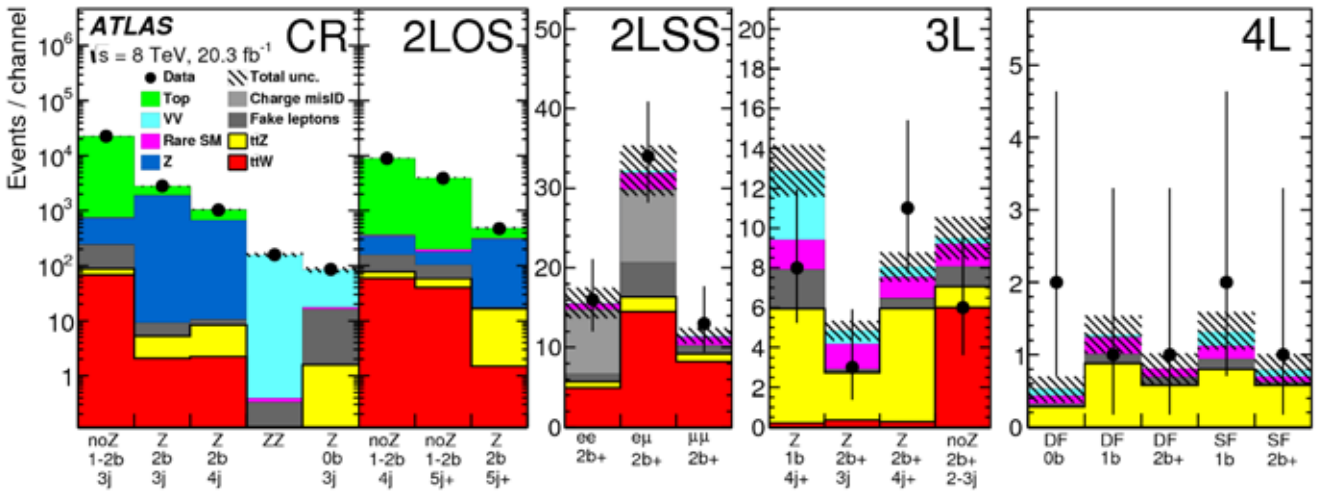

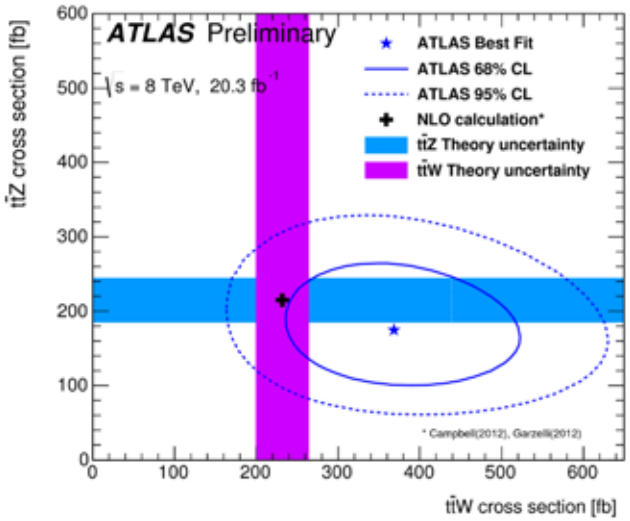

V.5.3 Single Top Production

- Single top was discovered by CDF and D0 in 2009
- *t*-channel production dominates over *s*-channel
- Study *t*-channel in *tq* mode with $t \to \ell \nu b$
- Use NN to separate signal from background (7 inputs)
- See significant signals

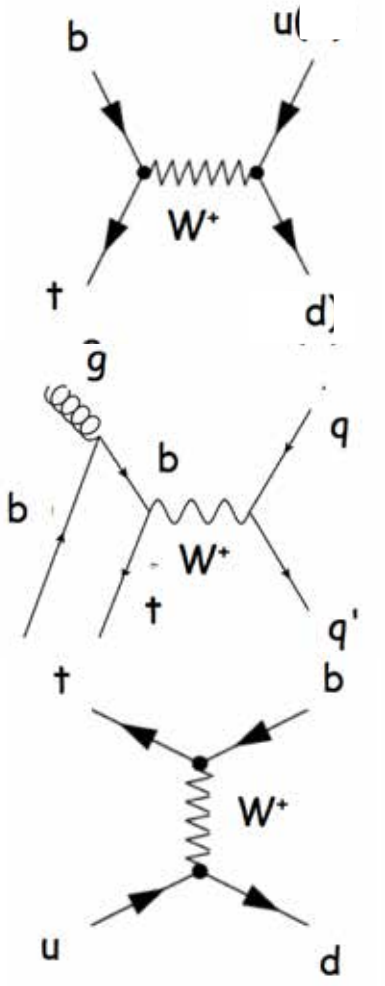

Process	$\hat{\nu}(\ell^+)$	$\hat{\nu}(\ell^-)$
tq	11 800 ± 200	17 ± 1
$\bar{t}q$	11 ± 1	6 920 ± 170
$t\bar{t}, Wt, t\bar{b}/\bar{t}b$	19 300 ± 740	18 900 ± 730
W^+ + jets	18 800 ± 780	48 ± 2
W^- + jets	23 ± 1	13 100 ± 740
Z, VV + jets	1 290	1 190
Multijet	4 520	4 520
Total estimated	55 800 ± 1 100	44 700 ± 1 100
Data	55 800	44 687

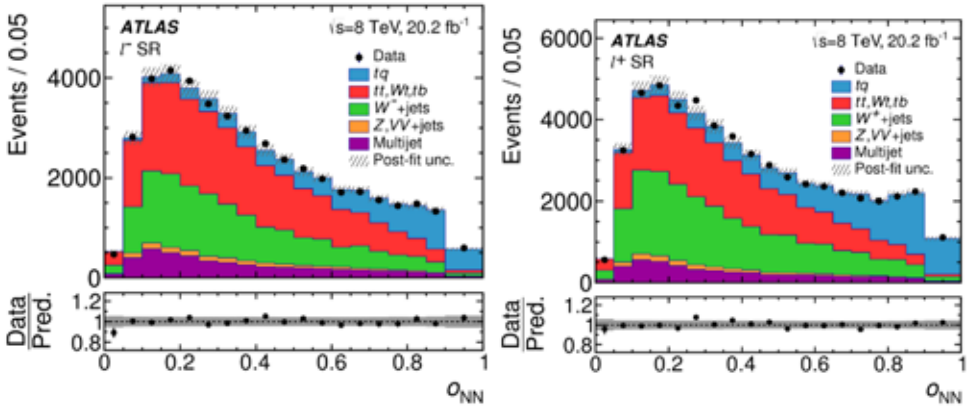

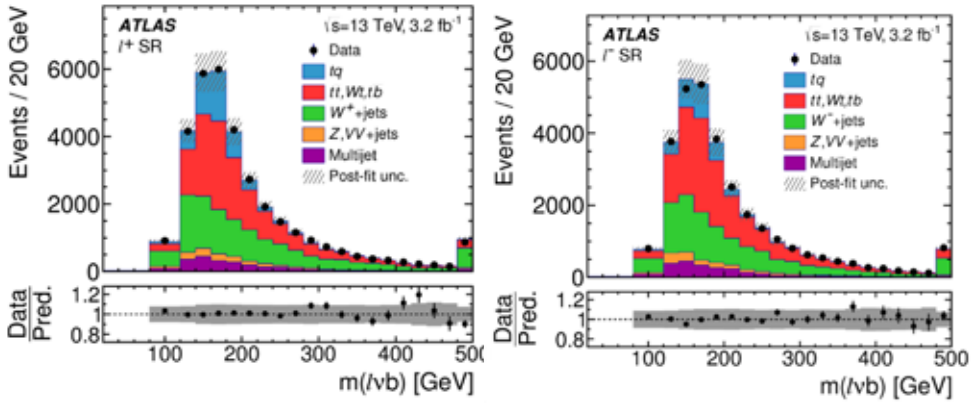

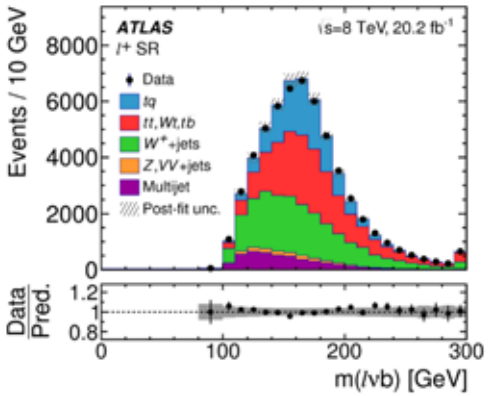

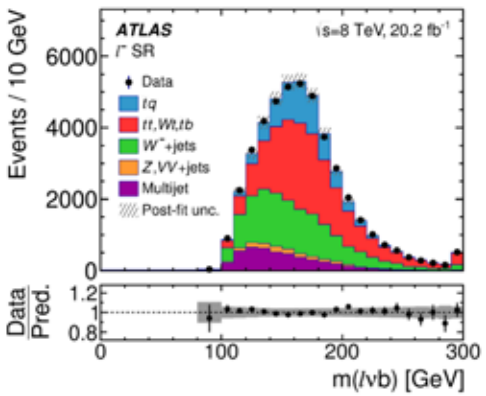

V.5.3 Single Top Production

- ATLAS observes single top production in the s-channel at 3.2 s.d.
- ATLAS measures the cross sections in the *t*-channel and *s*-channel at 8 TeV: ATLAS NLO SM prediction

t-channel

$\sigma_{tot}(tq) = 56.7^{+4.3}_{-3.8}\,pb$ (5.42) $\sigma_{tot}(t\bar{q}) = 54.9^{+2.3}_{-1.9}\,pb$ (5.43)

$\sigma_{tot}(\bar{t}q) = 32.9^{+3.0}_{-2.7}\,pb$ (5.44) $\sigma_{tot}(\bar{t}\bar{q}) = 29.7^{+1.7}_{-1.5}\,pb$ (5.45)

s-channel

$\sigma_s = 4.8^{+1.8}_{-1.5}\,pb$ (5.46) $\sigma_s^{th} = 5.61 \pm 0.22\,pb$ (5.47)

- Measurements are in good agreement with the NLO SM prediction
- From $\sigma_{tot}(t\bar{q}+\bar{t}q)$ determine $|V_{tb}|$

$|V_{tb}| = 0.88 \pm 0.07$ (5.48)

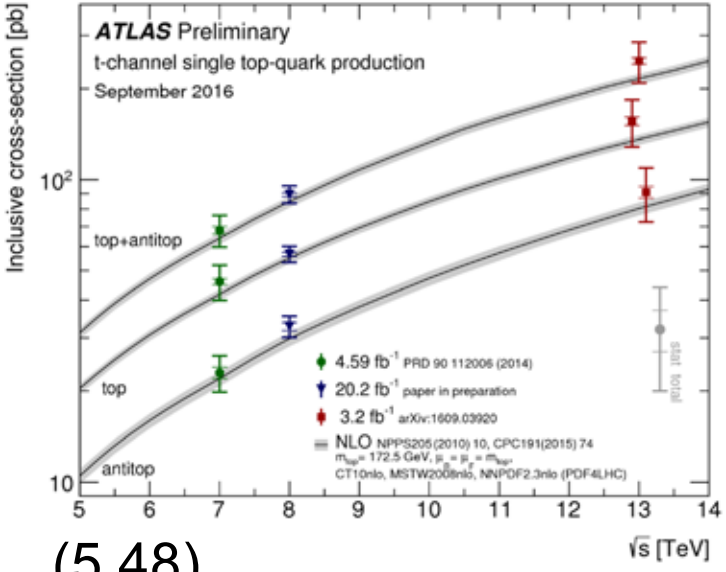

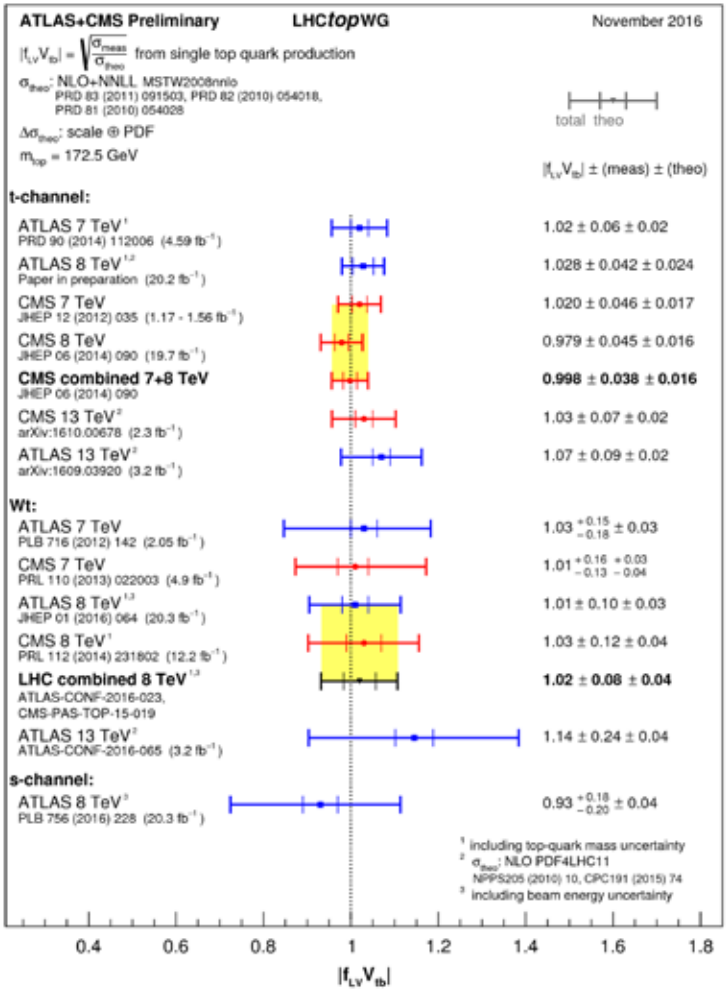

- $|V_{tb}|$ measurements are consistent with 1 but errors are still large

V.6 Observables at Hadron Colliders

- In hadron colliders, we characterize processes by kinematic variables: transverse momentum p_T, azimuth angle ϕ and pseudorapidity η

$$\eta = -\ln\left(\tan\left[\theta/2\right]\right) \tag{5.49}$$

- For masses much smaller than p_T, pseudorapidity and rapidity are equal

where rapidity is defined as $$y = \frac{1}{2}\ln\left(\frac{E + p_{\|}}{E - P_{\|}}\right) \tag{5.50}$$

- The separation between two objects *i* and *j* in the $\eta - \phi$ plane is

$$\Delta R_{i,j} = \sqrt{\left(\eta_i - \eta_j\right)^2 + \left(\phi_i - \phi_j\right)^2} \tag{5.51}$$

- Using these variables we define the transverse mass

$$E^2 - p_{\|}^2 = m^2 + p_T^2 \equiv m_T^2 \tag{5.52}$$

- Thus, $$E = m_T \cosh y \tag{5.53}$$

- The maximum value of *y* at fixed E occurs at p_T=0, cosh y_{max}=γ, yielding y_{max}=7.7 for the Tevatron (2 TeV) and y_{max}=9.6 for LHC (14 TeV)

V.6.1 Observables at Hadron Colliders: Rapidity

- Gluon-gluon scattering is one of the dominant subprocesses in proton-proton collisions

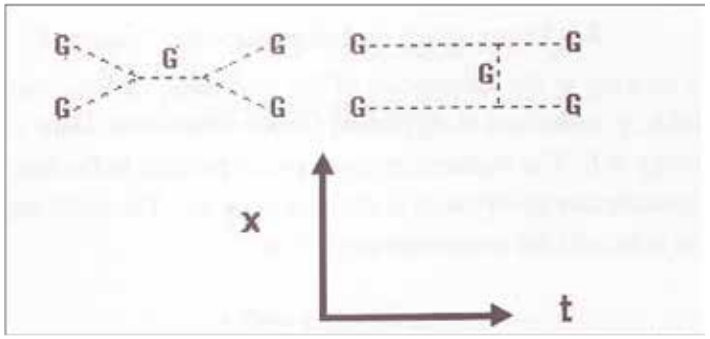

- The rapidity distribution at 14 TeV shows a flat plateau of width $\Delta y = \pm 3$

- This indicates that the produced particles follow single particle phase space at wide angles

- The ATLAS coverage is
  $\Delta y = \pm 2.7$ muon system,
  $\Delta y = \pm 4.9$ em calorimeter
  $\Delta y = \pm 2.5$ tracking

- At the Tevatron at 1.96 TeV the plateau is only $\Delta y = \pm 2$

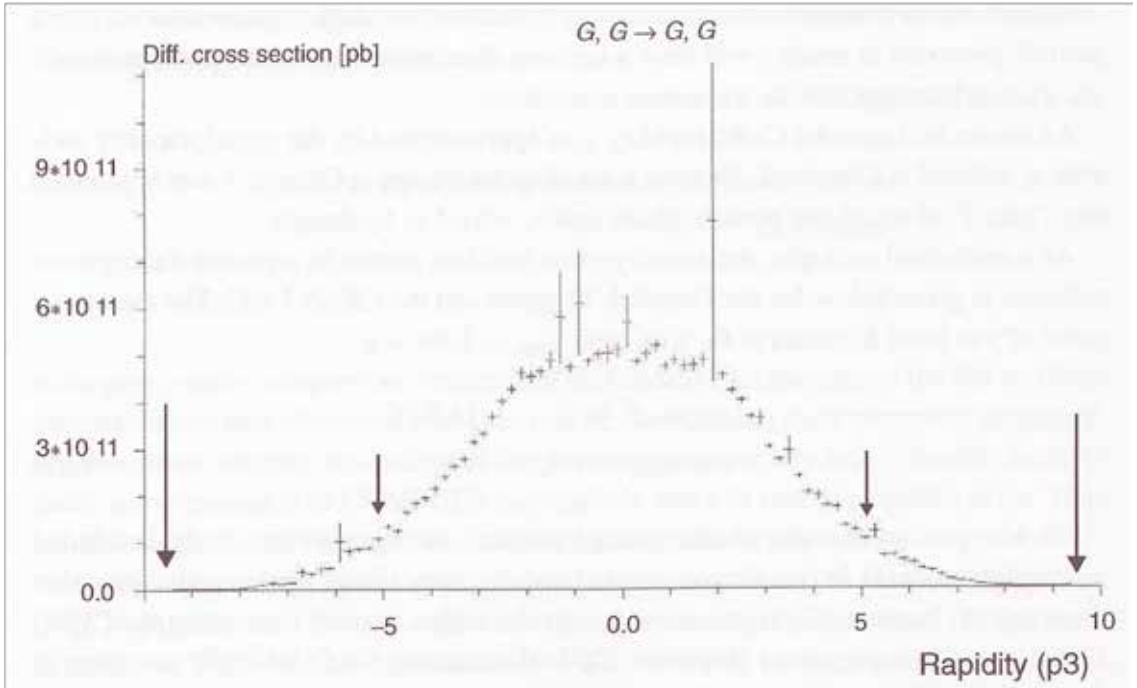

Figure 3.2 Rapidity distribution for produced gluons at the LHC (14 TeV p–p CM energy). The small arrows indicate the limits of the angular coverage of the detector shown in Chapter 2. The larger arrows indicate the initial proton beam rapidity in the CM.

V.6.2 Jet Characteristics

- The jet production cross section depends on η, showing a steeper E_T dependence for large η
- We assume that the *p* is an incoherent sum of *u* & *d* valence quarks, radiated *g* plus a sea of $q\bar{q}$ pairs
- The reason is that 2 fundamental scales contribute here: the binding energy scale or size of proton and the hard or fundamental collision scale
- We operate at hard scale, $p_T \gg \Lambda_{QCD}$, since p will dissociate into partons with life time $1/\Lambda_{QCD}$ long wrt $1/p_T$

  ➔ incoherent scattering

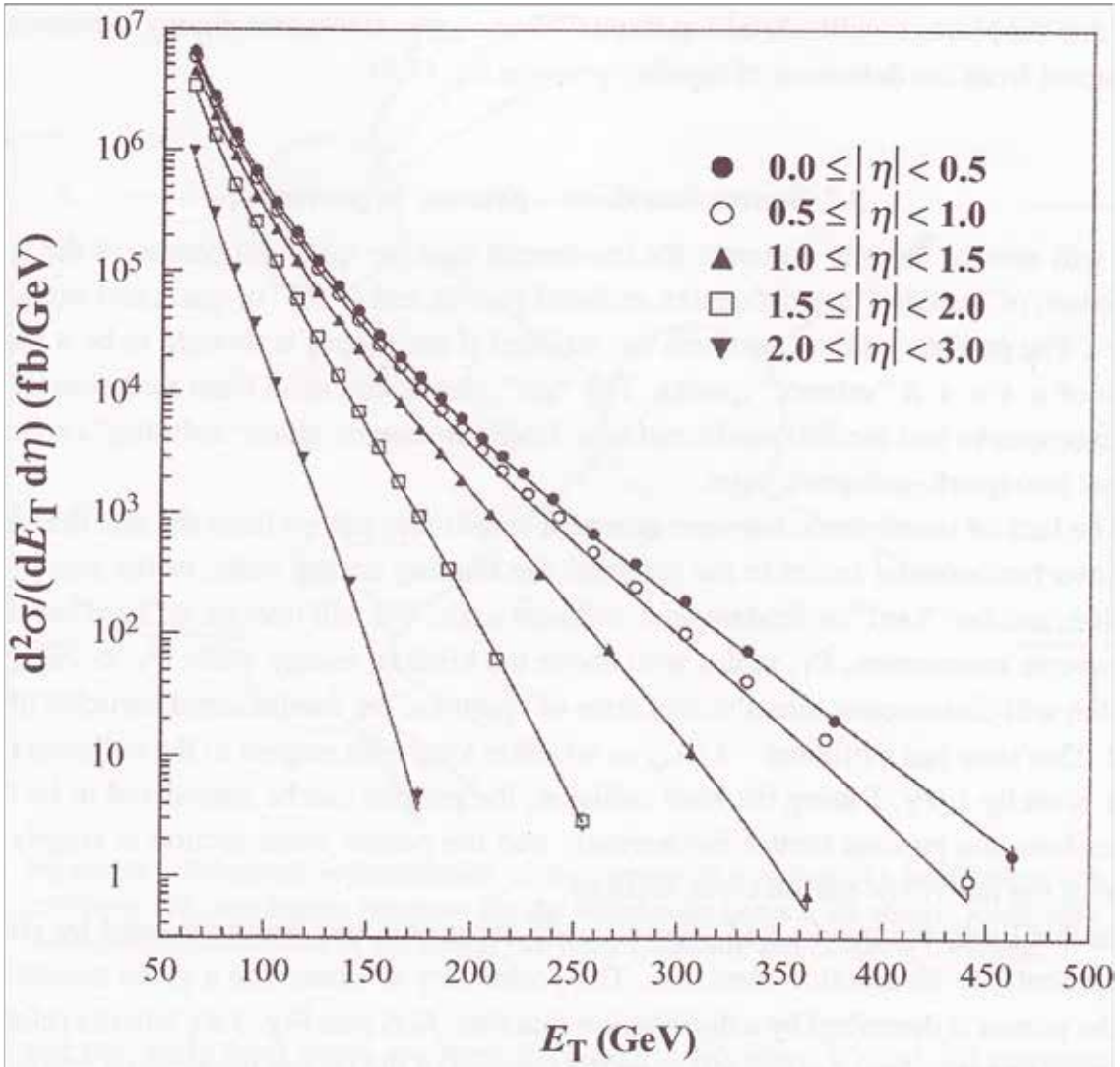

Figure 3.3 D0 data for the jet cross section in different pseudorapidity ranges as a function of transverse energy of the jet ([1] – with permission). The lines represent different distribution function fits.

V.6.2 Jet Characteristics

- Inclusive jet double differential cross section from ATLAS at 13 TeV

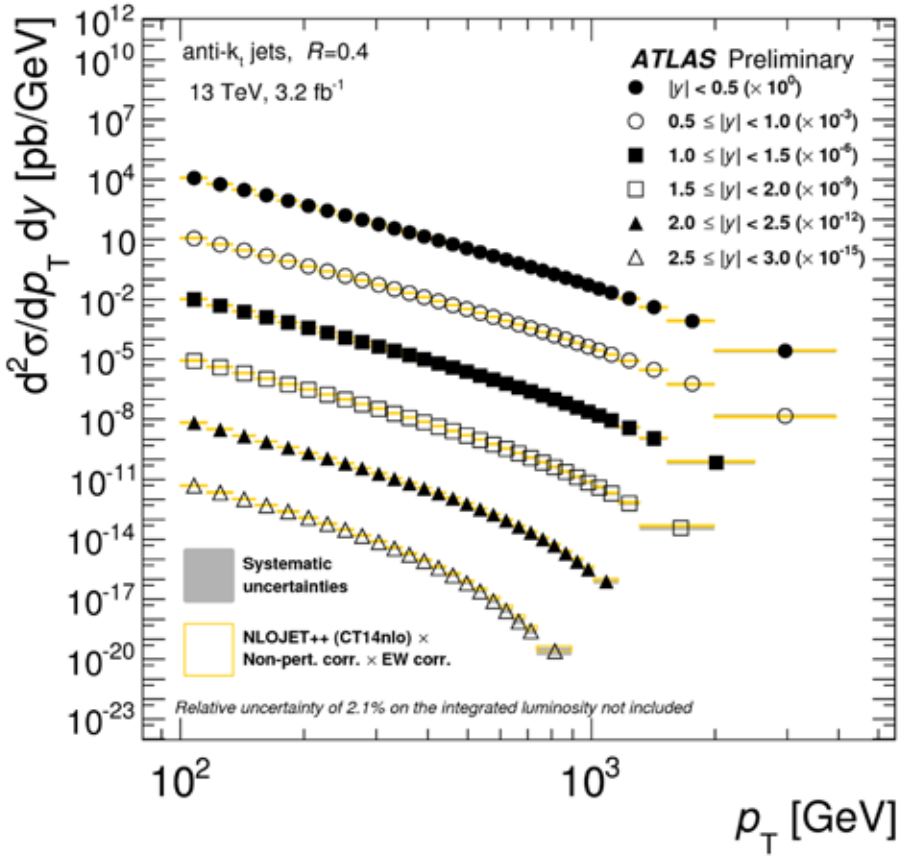

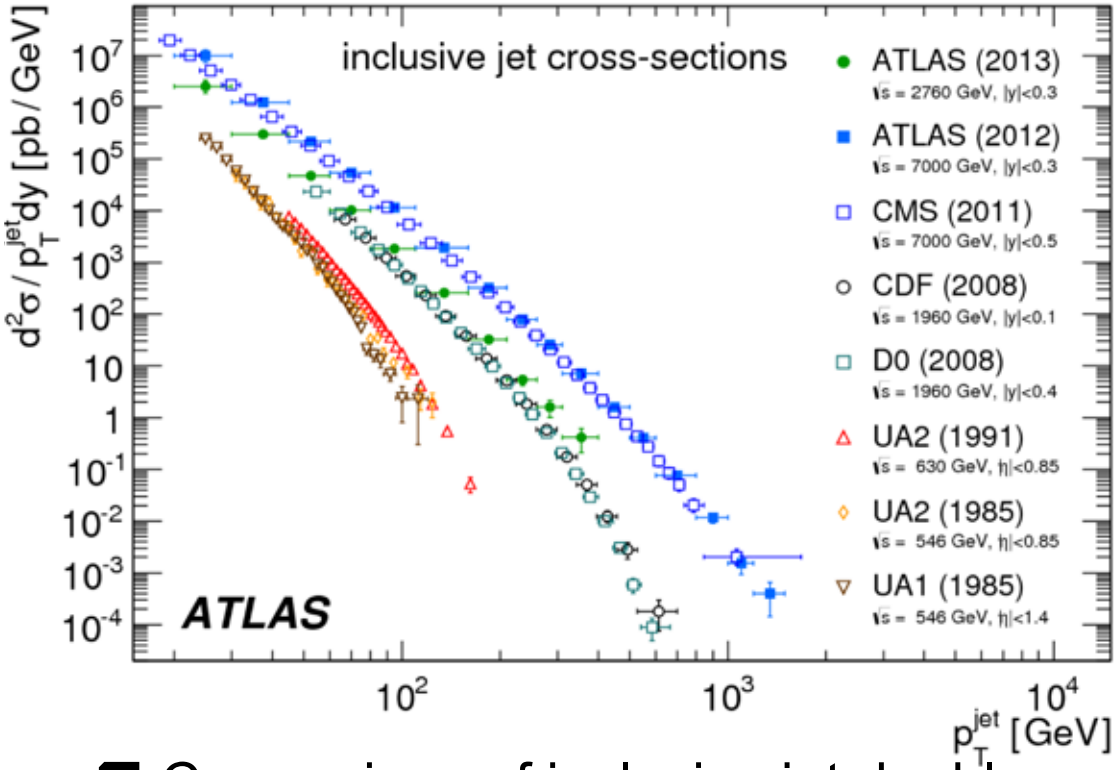

- Comparison of inclusive jet double differential cross sections from different experiments at different energies

- At large η, the differential cross section falls off faster at high p_T; At low p_T slopes are similar for different η
- Data are well described by prediction

V.6.2 Jet Characteristics

- In hadron-hadron collisions typically two partons interact and remaining partons produce the **U**nderlying **E**vent
- They evolve into soft pions (p_T~0.4 GeV) with a charge density of 6 per unit rapidity in a ratio of $\pi^{\pm}:\pi^0$=2:1
- Every interaction will contain a similar distribution of "soft" or low transverse momentum particles, called minimum bias events
- A clear plateau in η is visible rising slowly with $\sqrt{s}$; its width increases with $\sqrt{s}$
- The p_T distribution is tightly localized to values < 0.5 GeV and $\sqrt{s}$ dependence for p_T < 1 GeV is small
- We can fit the p_T behavior with

$$\frac{d^3\sigma}{\pi dy dp_T^2} \sim \frac{A}{(p_T + p_0)^n} \qquad (5.54)$$

A~450 mb/GeV^2, p_0~1.3 GeV, n~8.2

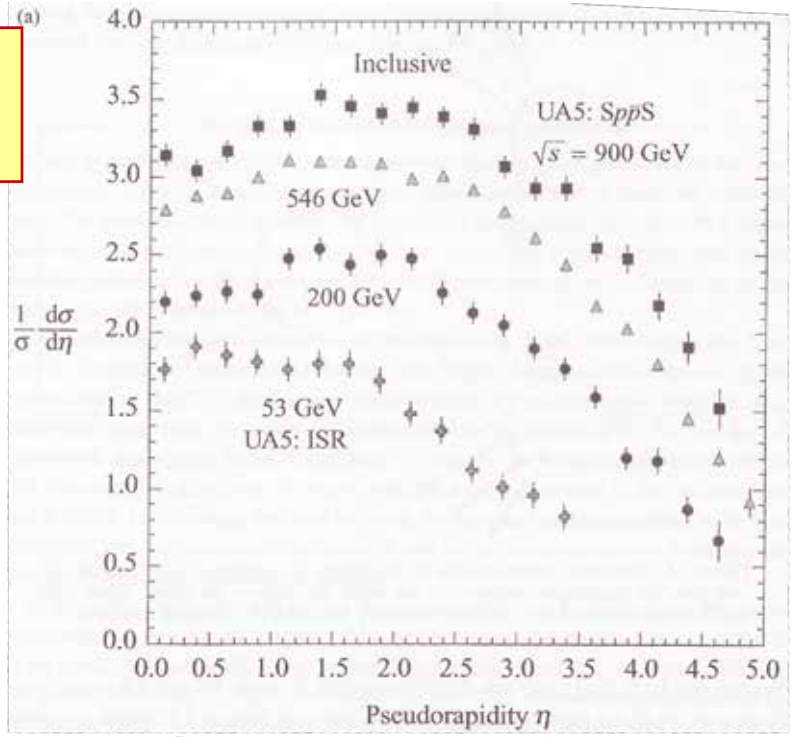

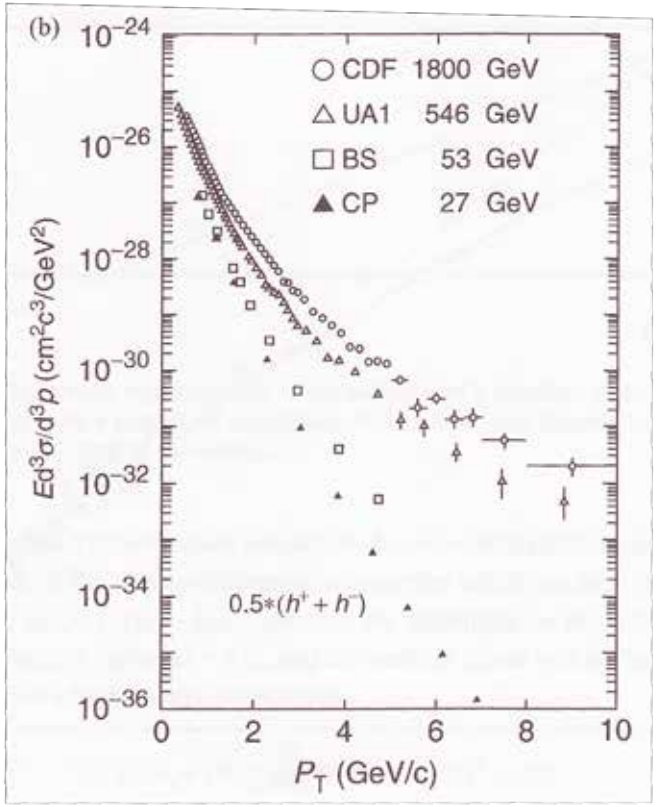

V.6.2 Jet Characteristics

- The coefficient A is of $\mathcal{O}$(100 mb)
  ➔ since this is of the order of total inelastic cross section; the low p_T particles make the bulk of particles produced in inelastic p-p interactions
- For $p_T \gg p_0$ cross section drops as p_T^n, large n
- The fragments of hadrons A and B at low p_T merge smoothly with fragmentation products of minijets for p_T > 10 GeV

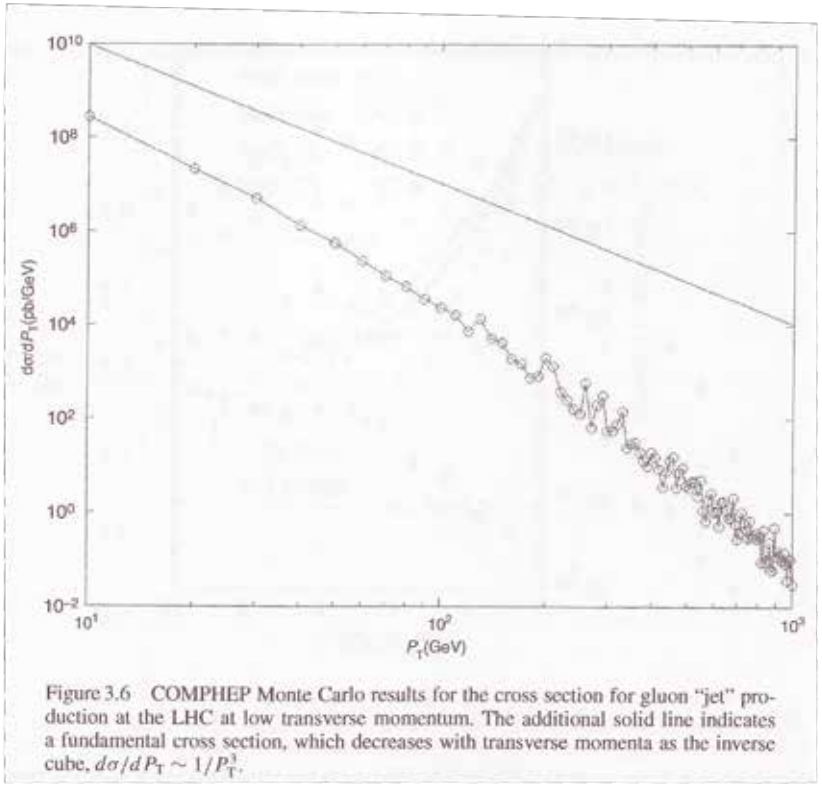

Figure 3.6 COMPHEP Monte Carlo results for the cross section for gluon "jet" production at the LHC at low transverse momentum. The additional solid line indicates a fundamental cross section, which decreases with transverse momenta as the inverse cube, $d\sigma/dP_T \sim 1/P_T^3$.

- Production of g jets has cross section of ~1 mb at p_T ~10 GeV
- Boundary between soft and hard physics is not very definite
- Simulation shows expected cross section for g-g scattering at the LHC at 14 TeV

V.6.3 Distribution Functions

- Thus, quarks and gluons inside proton can be represented by classical distribution functions $f^A_i(x)$, where x is momentum fraction

- If we had only 3 valence quarks their distribution functions would be expected to peak at x=1/3

- Since u &d quark masses are 5 MeV compared to m_p=940 MeV, quark motion is relativistic
  ➔ radiated gluons which have small x distribution

- The gluons themselves can split or decay to $q\bar{q}$, thus apart from $u\bar{u}$, $d\bar{d}$, also $s\bar{s}$ and $c\bar{c}$ pairs may be created at very small x

$$\int_0^1 dx\ u_v(x) = 2, \quad \int_0^1 dx\ d_v(x) = 1 \qquad (5.55)$$

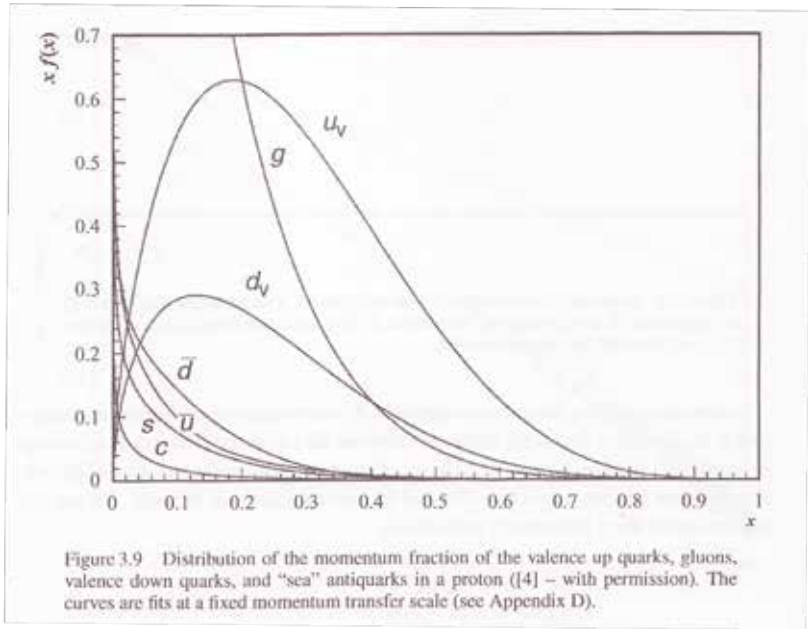

Figure 3.9 Distribution of the momentum fraction of the valence up quarks, gluons, valence down quarks, and "sea" antiquarks in a proton ([4] – with permission). The curves are fits at a fixed momentum transfer scale (see Appendix D).

Parton functions

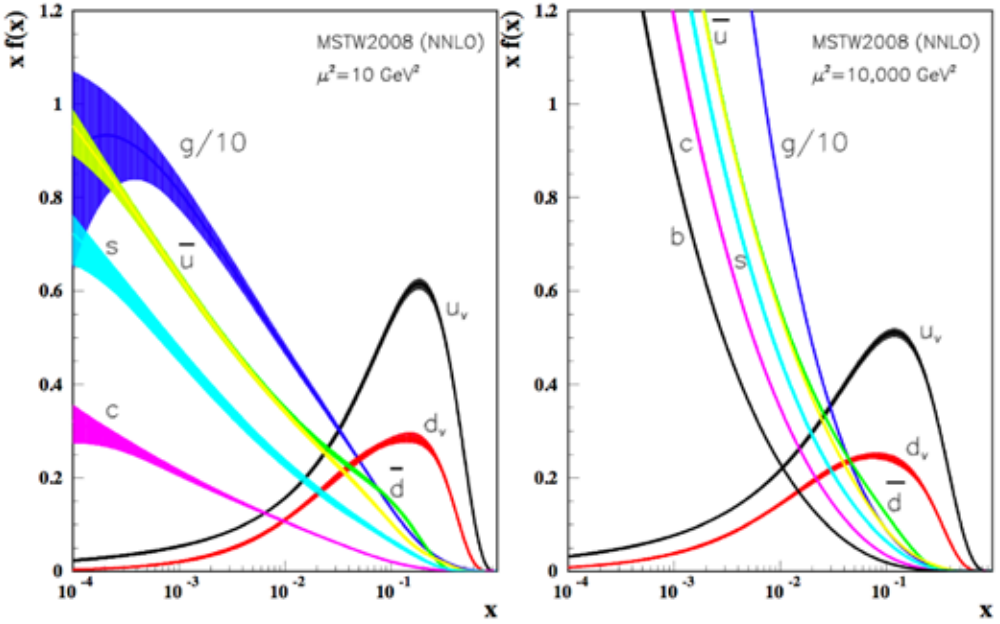

V.6.3 Distribution Functions

- We note that valence and sea quarks carry half the momentum

$$\sum_q \int_0^1 dx\ x\left(q(x)+\bar{q}(x)\right) \simeq 0.5 \qquad (5.56)$$

- The other half is carried by gluons

$$\int_0^1 dx\ x\cdot g(x) \simeq 0.5 \qquad (5.57)$$

- This is confirmed experimentally in lepton scattering experiments

- Suppression at high x is ensured by

$$xg(x) = \tfrac{7}{2}(1-x)^6 \qquad (5.58)$$

- The pointlike cross section for pointlike scattering of partons is

$$\hat{\sigma} \sim \pi\alpha_1\alpha_2 \frac{|A|^2}{\hat{s}} \qquad (5.59)$$

where α_1 and α_2 are the couplings at the 2 vertices and the amplitudes for the various processes are shown in the table below

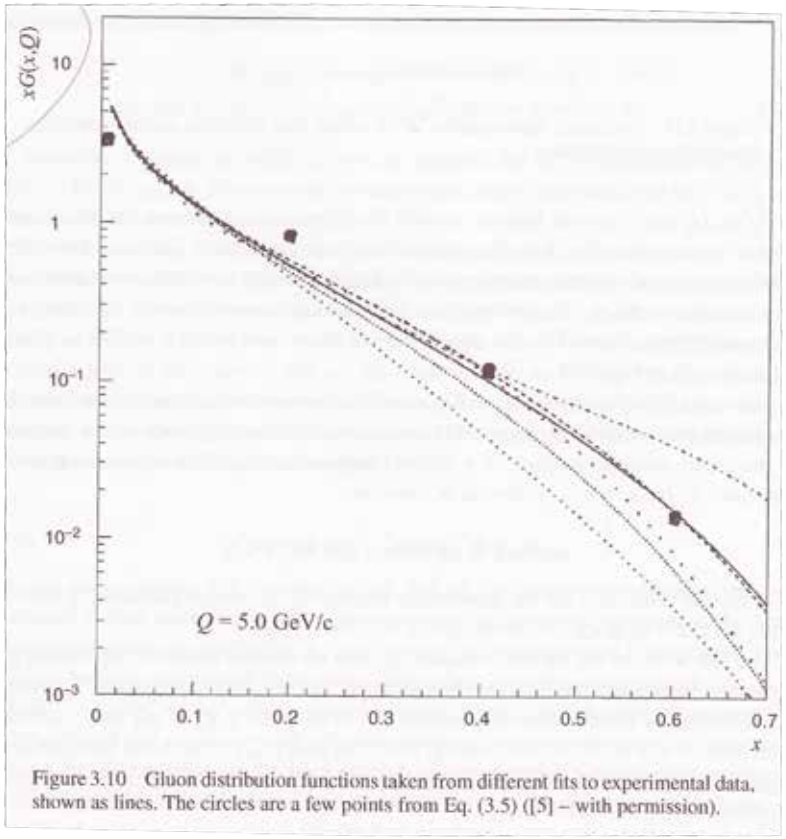

Figure 3.10 Gluon distribution functions taken from different fits to experimental data, shown as lines. The circles are a few points from Eq. (3.5) ([5] – with permission).

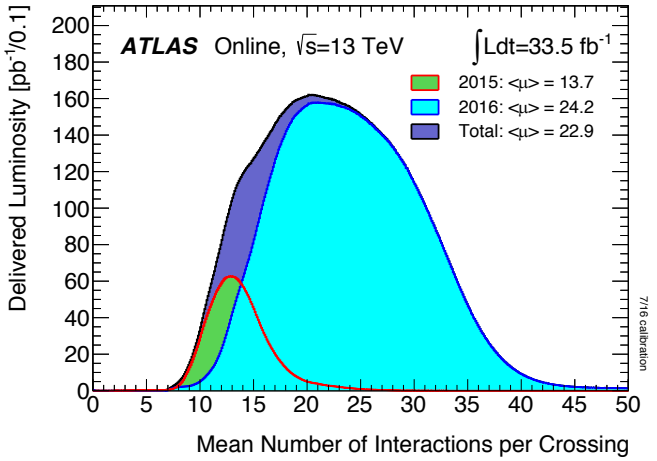

V.6.4 Pointlike Scattering of Partons

- For $\mathcal{L}$~10^{34}/(cm^2 s) & σ~100 mb at the LHC, total inelastic rate is $\sigma \cdot L$~1GHz
  - ➔ for 25 ns beam Xing expect 25 minimum bias events/Xing
- g-g scattering has by far the largest cross section (>5 times)
- While final-state particles like e, μ, γ appear directly in the detector, quarks and gluons appear as jets

Table 3.1 *Point like cross sections for parton–parton scattering. The entries have the generic dependence of Eq. (3.10) already factored out. At large transverse momenta, or scattering angles near 90 degrees ($y \sim 0$), the remaining factors are dimensionless numbers of order one ([4] – with permission).* (there should be a ˆ on *s*, *t*, *u*)

Process	$\lvert A\rvert^2$	Value at $\theta = \pi/2$
$q + q' \to q + q'$	$\frac{4}{9}[s^2 + u^2]/t^2$	2.22
$q + q \to q + q$	$\frac{4}{9}[(s^2 + u^2)/t^2 + (s^2 + t^2)/u^2] - \frac{8}{27}(s^2/ut)$	3.26
$q + \bar{q} \to q' + \bar{q}'$	$\frac{4}{9}[t^2 + u^2]/s^2$	0.22
$q + \bar{q} \to q + \bar{q}$	$\frac{4}{9}[(s^2 + u^2)/t^2 + (t^2 + u^2)/s^2] - \frac{8}{27}(u^2/st)$	2.59
$q + \bar{q} \to g + g$	$\frac{32}{27}[t^2 + u^2]/tu - \frac{8}{3}[t^2 + u^2]/s^2$	1.04
$g + g \to q + \bar{q}$	$\frac{1}{6}[t^2 + u^2]/tu - \frac{3}{8}[t^2 + u^2]/s^2$	0.15
$g + q \to g + q$	$-\frac{4}{9}[s^2 + u^2]/su + [u^2 + s^2]/t^2$	6.11
$g + g \to g + g$	$\frac{9}{2}[3 - tu/s^2 - su/t^2 - st/u^2]$	30.4
$q + \bar{q} \to \gamma + g$	$\frac{8}{9}[t^2 + u^2]/tu$	
$g + q \to \gamma + q$	$-\frac{1}{3}[s^2 + u^2]/su$	

- The process from parton to jets is called fragmentation ➔ it is a complex process simulated in various computer programs (PYTHIA, HERWEG, ISAJET)

V.6.5 Jet Fragmentation

- Assume fragmentation properties factorize ➔ parent quark or gluon fragment is independent of the mechanism parent is created ➔ we need only a single unified description of fragmentation process
- # particles in jet depends logarithmically on parent particle momentum
- Assume: all fragments are pions (simplicity)
- Assume: p_T acquired in the fragmentation process is limited to the fragment momentum transverse to parent jet axis, $k_T \sim \Lambda_{QCD}$
- The fragmentation function $D(z)$ describes the distribution in $z=k/P$ of those products in which z is the momentum fraction of the parent with momentum P, carried off by the fragment with momentum k
- The fraction z is bounded by $M_\pi / P < z < 1$

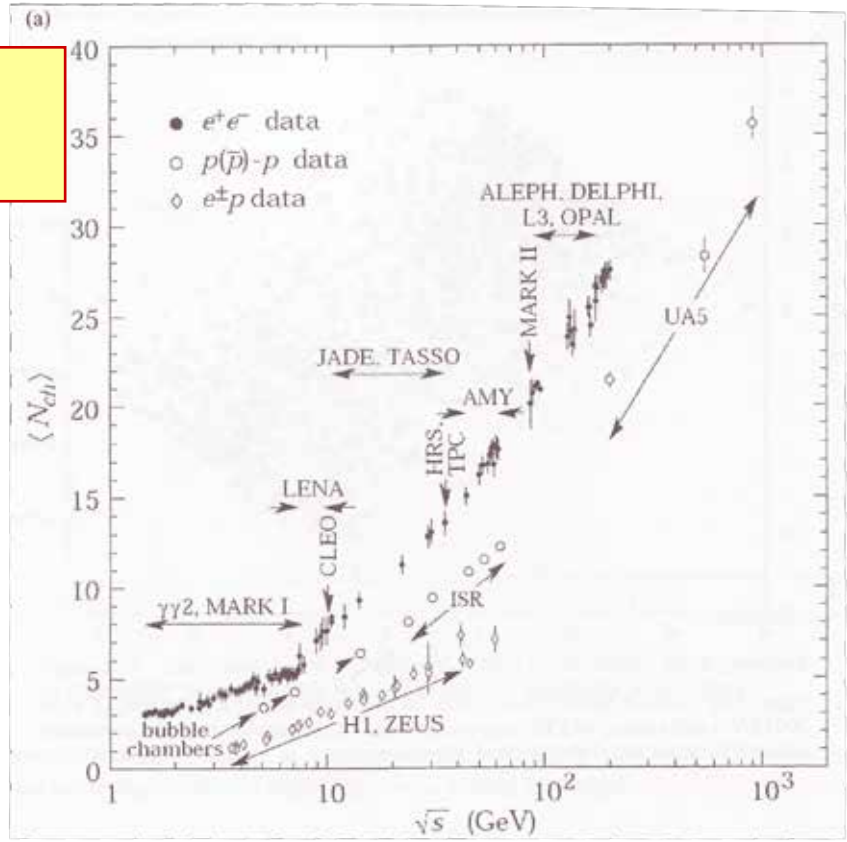

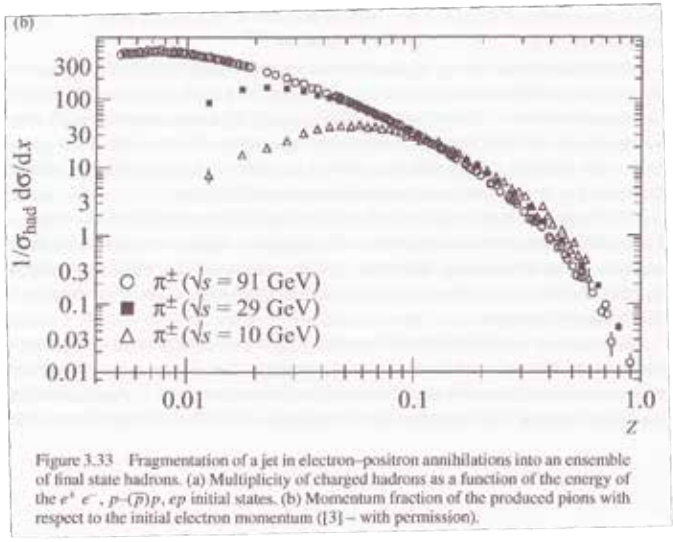

Figure 3.33 Fragmentation of a jet in electron–positron annihilations into an ensemble of final state hadrons. (a) Multiplicity of charged hadrons as a function of the energy of the e^+e^-, p–$(\bar{p})p$, ep initial states. (b) Momentum fraction of the produced pions with respect to the initial electron momentum ([3] – with permission).

V.6.5 Jet Fragmentation

- It has a radiative form similar to that already assumed for the parton distribution functions

- We get $zD(z) = a(1-z)^{\alpha}$ (5.60)

from which we determine the multiplicity

$$\langle n \rangle = \int D(z)dz \sim a \int_{M_\pi/P}^{1} dz/z \sim a\ln(P/M_\pi) \quad (5.61)$$

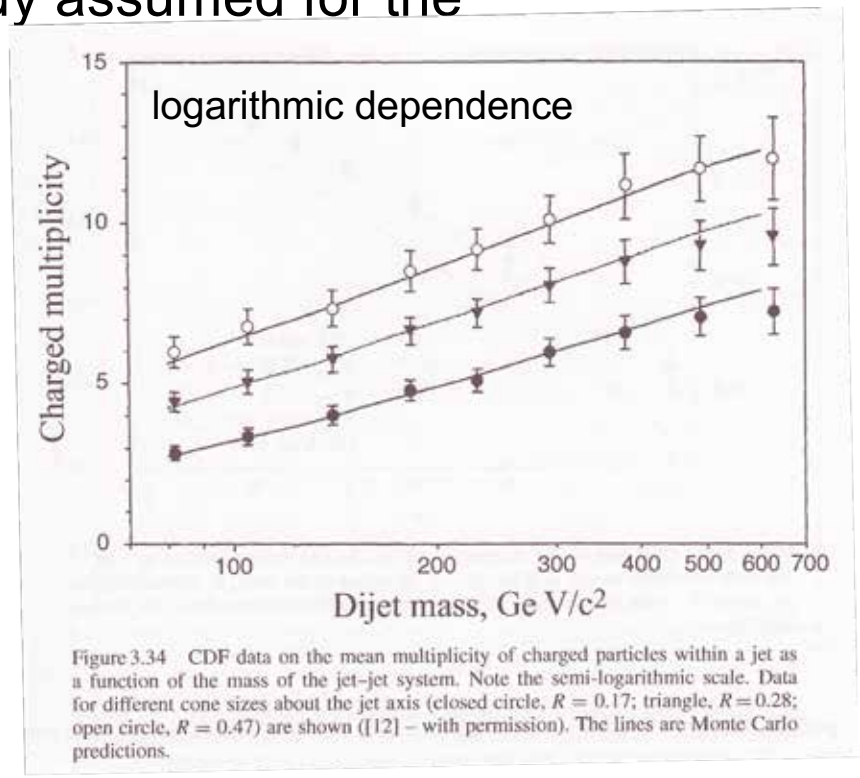

Figure 3.34 CDF data on the mean multiplicity of charged particles within a jet as a function of the mass of the jet–jet system. Note the semi-logarithmic scale. Data for different cone sizes about the jet axis (closed circle, $R = 0.17$; triangle, $R = 0.28$; open circle, $R = 0.47$) are shown ([12] – with permission). The lines are Monte Carlo predictions.

- The fragmentation process implies that we observe a jet of particles that moves approximately along the direction of the parent quark or gluon

- We expect a core within the jet that carries most of the jet momentum and that is localized at a small cone radius, R, in (η, ϕ) space

$$R = \sqrt{\Delta\eta^2 + \Delta\phi^2} \quad (5.62)$$

V.6.5 Jet Fragmentation

- The core is surrounded at larger R by many low-energy particles
- From the CDF data it is evident that a sharply peaked distribution of particles around the jet axis exists, as the multiplicity increases less than linear
- In the CDF plot shown on RH side we see 40% of the energy of the jet contained in a cone with R=0.1, while 80% is contained in a cone with R=0.4
- In simulations of the data using $zD(z)=(1-z)^5$ and $\langle k_T \rangle \sim 0.72$ GeV the highest jet energy is about 1/4 of the jet momentum
- Fragmentation is soft introducing non-perturbative effects

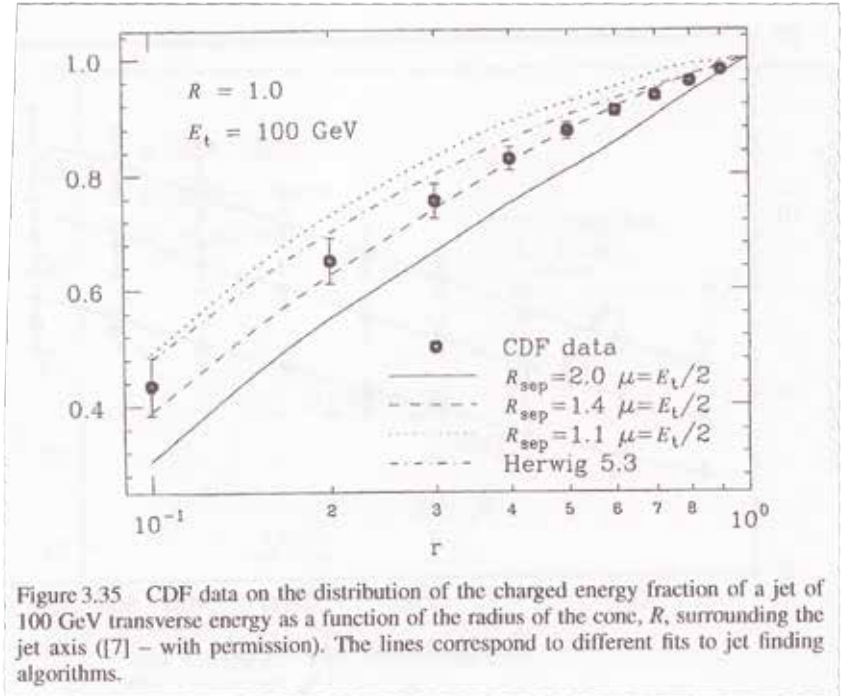

Figure 3.35 CDF data on the distribution of the charged energy fraction of a jet of 100 GeV transverse energy as a function of the radius of the cone, R, surrounding the jet axis ([7] – with permission). The lines correspond to different fits to jet finding algorithms.

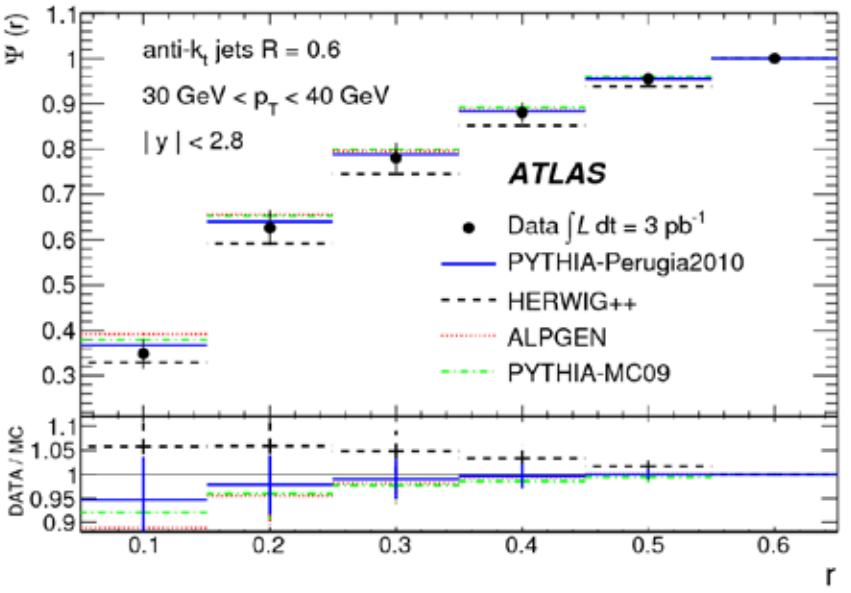

V.6.2 Event Shape Observables

- In pp collisions we have to deal with the **U**nderlying **E**vent since typically 2 partons interact and the remaining partons form the UE (jets)
- Event shape variables are used to separate signal from backgrounds
- Lets look at common event shape variable in $Z^0 \to \mu^+\mu^-$
  - number of charged tracks ➔ multiplicity increases with dimuon p_T
  - Scalar sum of p_T :
    ➔ increases with dimuon p_T, long tail
  - Beam thrust:
    ➔ increases with dimuon p_T, long tail

$$\sum_i \left|\hat{p}_T^i\right| = \sum p_T \qquad (5.63)$$

$$\mathcal{B} = \sum_i p_T^i \exp[-|\eta_i|] \qquad (5.64)$$

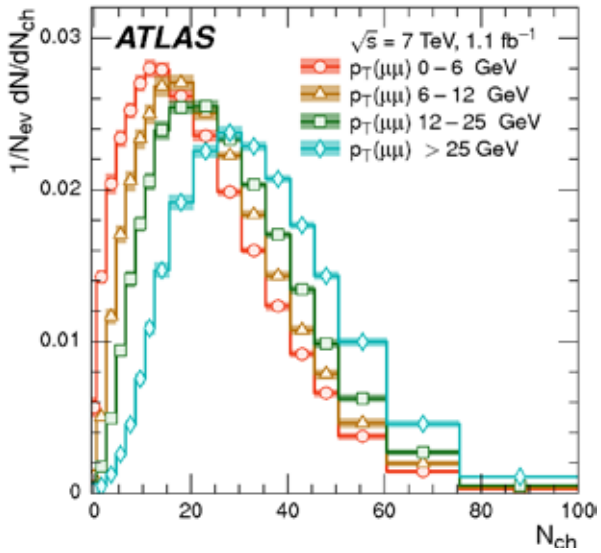

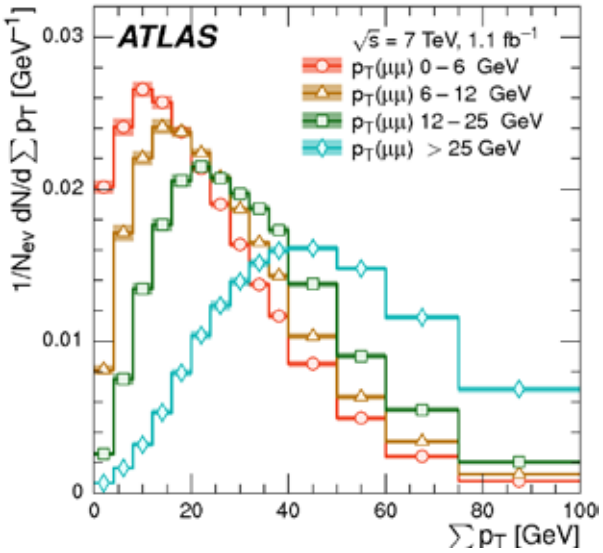

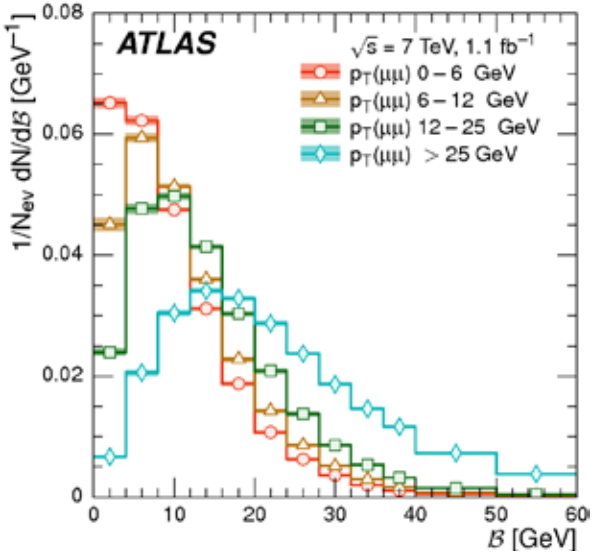

V.6.2 Event Shape Observables

- Thrust:
  - ➔ increases with dimuon p_T

$$\mathcal{T} = \max_{\hat{n}_T} \frac{\sum_i \left|\vec{p}_T^{\,i} \cdot \hat{n}_T\right|}{\sum_i \left|\vec{p}_T^{\,i}\right|} \qquad (5.65)$$

- Spherocity:
  - ➔ becomes more symmetric with larger dimuon p_T

$$S = \frac{\pi^2}{4} \min_{\vec{n}=(n_x,n_y,0)^T} \left(\frac{\sum_i \left|\vec{p}_T^{\,i} \times \vec{n}\right|}{\sum_i \left|p_T^i\right|} \right)^2 \qquad (5.66)$$

- *F* parameter is defined as ratio of smaller to larger eigenvalues of the transverse momentum tensor

- For high dimuon p_T different prediction yield reasonable description